Cooling performance of an active-passive hybrid composite phase change material (HcPCM) finned heat sink: Constant operating mode

Adeel Arshad[a,*], Syed Atif Iqrar[b], Sol Carolina Costa Pereira[c], Muhammad Wakil Shahzad[c], Kashif Nawaz[d], William Worek[e,*]

[a]*Environment and Sustainability Institute (ESI), Faculty of Environment, Science and Economy, University of Exeter, Penryn Campus, Cornwall, TR10 9FE, United Kingdom*
[b]*College of Engineering and Physical Sciences, Aston Institute of Photonic Technologies, Aston University, Birmingham, B4 7ET, United Kingdom*
[c]*Department of Mechanical and Construction Engineering, Faculty of Engineering and Environment, Northumbria University, Newcastle upon Tyne, NE1 8ST, United Kingdom*
[d]*Building and Transportation Science Division, Oak Ridge National Laboratory, Oak Ridge, 37830, Tennessee, United States*
[e]*Building and Industrial Technologies Energy Systems and Infrastructure Analysis Division, Argonne National Laboratory, Lemont, IL 60439, United States*

Abstract

The present study explores a hybrid thermal management technology based on air cooling and hybrid composite phase change material (HcPCM) filled finned heat sink for cooling performance of lower to medium heat flux dissipating electronic devices. Two-dimensional numerical simulations are conducted to study the conjugate heat transfer effects of three types of finned heat sink: air-cooled finned heat sink, HcPCM-cooled finned heat sink, and hybrid (air-HcPCM) cooled finned heat sink. A heat sink with a constant volume faction of plate-fins is designed in all cases and simultaneous effects of hybrid nanoparticles and air are investigated to keep the heat sink temperature at safe operating conditions between $40-60$ °C. The effect of air is incorporated into the heat sink by applying the convective heat transfer coefficient of $h_c = 10-100$ W/m^2.K which tends to create the natural convection and forced convection heat transfer characteristics. The heat flux is varied from $25-40$ kW/m^2 in the current study. The hybrid nanoparticles of carbon additives (GO and MWCNTs) are dispersed into the RT-35HC, used as a PCM, with a volume fraction of 0% to 6%. Transient simulations are carried out using COMSOL Multiphysics to solve the governing equations for PCM based conjugate heat transfer model. The results showed that forced convection heat transfer improved the cooling performance of the hybrid heat

*Correspondence author:
Email addresses: `a.arshad@exeter.ac.uk`, `adeel_kirmani@hotmail.com` (Adeel Arshad), `wworek@anl.gov` (William Worek)

sink compared to natural convection heat transfer. The addition of nanoparticles further enhanced thermal enhancement and uniform melting distribution of PCM inside the finned heat sink. The h_c between 30 to 50 $W/m^2.K$ shows optimized values for forced convection heat transfer operating conditions. The volume fraction of 2% of GO+MWCNTs nanoparticles in recommended or optimum concentration for uniform melting of PCM inside the finned heat sink.
Keywords: Hybrid composite phase change material; HcPCM-based Finned heat sink; Hybrid (air-HcPCM) Finned heat sink; Carbon-additives; Electronics devices

Nomenclature

Abbreviations

GO Graphite oxide

MWCNTs Multi-walled carbon nanotubes

FEM Finite Element method

HS Heat sink

TM Thermal management

HcPCM Hybrid composite phase change material

PCM Phase change material

BDF Backward Differentiation Formula

PARDISO Parallel Direct Sparse Solver Interface

Symbols

A_m Mushy zone

B Boltzman constant (J/K)

ρc_p Volumetric heat capacity $(J/m^3.K)$

g Gravitational acceleration (m/s^2)

F Force (N)

H Height (mm)

k Thermal conductivity $(W/m.K)$

L Latent heat of fusion $(J/kg.K)$

m Mass (kg)

p Pressure (Pa)

S Source term in momentum equation

V Volume (m^3)

T Temperature (K)

t Time (sec)

V Velocity (m/s)

W Width (mm)

c_p Specific heat capacity $(J/kg.K)$

h_c Convective heat transfer coefficient $(W/m^2.K)$

ΔH Fractional latent-heat $(J/kg.K)$

$2D$ Two dimensional

Greek letters

φ Volume fraction

μ Viscosity (Pa.s)

β Thermal expansion coefficient (1/K)

f_l Liquid fraction

φ Volume fraction of TCE

q Heat flux

sf Shape factor

Subscripts

ini Initial

l Liquidus

s Solidus

m Melting

$cpcm$ Composite phase change material

$hcpcm$ Hybrid composite phase change material

np Nanoparticles

eff effective

ref Reference

x $x-$axis

y $y-$axis

1. Introduction

The growing development and advancement in nanotechnology, the integration and miniaturization of integrated circuits (ICs) has shifted to high-density, smarter and faster with high local heat generation during operation. According to Moore's law, the number of transistors in microprocessors are growing exponentially because of the advancement in semiconductor manufacturing technologies [1, 2]. The heat source (i.e., chip) is considered highly intensive in miniaturized ICs. Thus, local heat dissipation is expected to vary between 600 to 1000 W/cm^2 in the next decades [3]. As a consequence, the technical performance of ICs are diminished or even sometimes totally shut down if that internal heat generated is not properly dissipated to the atmosphere. Therefore, for a safe, effective, and reliable operation of micro ICs, the chip temperature or junction temperature (the temperature at the silicon die) should be lower than the threshold value of $85 - 125$ °C, depending on the type of circuit board [4, 5]. For this purpose, an efficient and reliable thermal management technology has become a must-have challenge beforehand. With the conventional solutions for thermal management of electronics devices including natural convection and forced convection, single/multi-phase active and passive cooling systems [6]. According to the contact of cooling fluid, the cooling methods are classified as (i) direct contact and (ii) indirect contact [7, 8], as shown in Fig. 1. Among different cooling methods, the air cooling with forced convection is commonly used because of its simple assembly and low-cost advantages compared to the liquid cooling with forced convection. In the last decade, the indirect cooling method based on phase change materials (PCMs) filled heat sink has introduced a new direction of heat dissipation from ICs as a passive cooling technique. With excellent inherent thermophysical properties such as high specific heat, high latent heat, constant phase-change temperature and good chemical stability of PCMs have proved a promising passive cooling medium for the eat dissipation of electronic equipment [9]. However, the lower thermal conductivities, paraffin-based PCMs, reduce the heat transfer rate during the charging and discharging modes of PCMs.

To enhance the heat transfer rate through the PCM, the researchers and scientists have adopted several approaches including extended surfaces [10–12], porous medium [13–15], and high thermal conductive nanomaterials, called as thermal conductivity enhancers (TCEs) [16–18]. The researchers further explored the effect of different geometric parameters of these TCEs individually. For instance Kandasamy et al. [19] conducted an experimental and numerical study for transient thermal management of plastic quad flat package (QFP) electronic devices using PCM based heat sink of 6, 10 and 33 plate-fins. The lower heat sink temperature was obtained with 33 plate-fin case. The higher discharging time was reported compared with the charging time at input power of 2, 3, and 4 W. Fok et al. [20] conducted an experimental study of plate-fins having 0, 3 and 6 number of fins of a PCM-filled heat sinks under different operation modes such as frequent, heavy and light usages. The lower

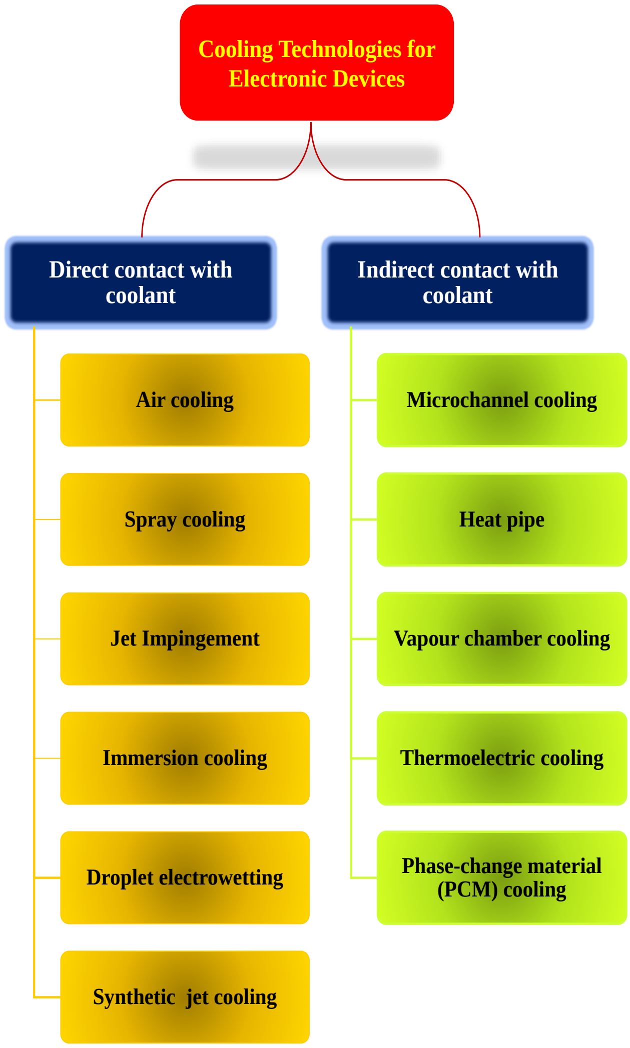

Figure 1: *Classification of commonly used thermal management methods [7, 8].*

heat sink base temperature and higher latent-heating phase completion duration were obtained with 6 number of plate-fin case. For all cases of usage, the less charging time of PCM was observed compared with the discharging time at different input power levels. Further, in another experimental study [21], they reported the charging time took approximately 120 mins whereas, partial solidification phase was achieved even after 250 mins of a PCM-filled heat sink at 5 W. Yang and Wang [22, 23] conducted a numerical study to validate the experimental results of [20, 21]. A good agreement in validation results with experimental data was achieved and only the results of the charging mode were presented. Baby and Balaji [24] investigated the PCM filled plate-fin and pin-fn configurations of constant volume fraction of 9% and found that pin-fin heat sink had better thermal performance compared with plate-fin heat sink filled with PCM. Further, they investigated the different number of fins of 33, 72 and 120 of PCM-based pin-fin heat sink [25]. The authors found the highest enhancement factor of 24 with 72 pin-fin heat sink filled with n-eicosane compared with a heat sink without fins at 7 W. The authors reported a charging time of 160 mins, whereas the discharging phase did not complete even after 270 mins. Mahmoud et al. [26] conducted an experimental study using 3, 6, 9, 36 and honeycomb cavities configuration PCM filled plate-fin heat sinks. The higher heat transfer performance was obtained with honeycomb configured PCM based heat sink during melting and cooling processes. The charging phase duration was reported as 60 mins at 3, 4 and 5 W, whereas the discharging phase took 160 mins to reach the ambient temperature at a 3 W power level. Arshad et al. [27] analyzed the impact of fin thickness on PCMs. According to the results, with the change of fin height, the volume fraction was also varied. The best cooling performance was obtained using 2 mm fin thickness at 1.0 volume fraction of PCM and also, number of fins have great impact on the effectiveness of PCM heat sinks. Further, they investigated the thickness of 2 mm square and 3 mm circular fins PCM heat sinks and found that 3 mm circular pin-fin PCM filled heat sink had the better thermal cooling performance [28, 29]. Ali et al. [30] experimentally investigated the different configurations such as triangular, rectangular and circular pin-fins heat sink filled with paraffin wax and n-eicosane filled. The authors revealed that triangular pin-fin configuration was the most effective compared with rectangular and circular pin-fins because of higher number fins and lower surface area ratio. Debich et al. [31] conducted a numerical study of a circular pin-fin heat sink filled with paraffin wax at a constant heat flux. The results of baseline and optimum designs are compared for both charging and discharging cases. It was found that the charging phase was completed after 120 min and discharging phase did not complete even after 140 mins. Deng et al.[32] conducted a comprehensive experimental study using plate-fin heats sink having 2, 4 and 6 number of fins at different heat fluxes. The authors found the complete charging and discharging in 90 and 410 mins, respectively. Mozafari and Lee [33] numerically studied the thermal cooling performance of a dual-PCM based heat sink. The n-eicosane and RT-44 were filled inside the plate-fin heat sink and results of charging and discharging were presented at constant heat flux. The complete charging of PCMs was reported after 64 mins whereas discharging time was reported of around 124 mins. Sivashankar and Selvam [34] conducted an experimental study based on different configurations of pin-fins such as circular, square, hexagonal and triangular and PCMs of different melting point temperatures namely, OM35 and OM46. It was reported that OM35 took 60 mins for charging duration, however, more than 200 mins were taken in discharging phase and it did not completely solidify. Kalbasi [35] conducted a numerical study to investigate the three different types of PCM-based plate-fin heat sinks under varying input power levels and different heat transfer coefficients. The author found that the performance of hybrid heat sink was acceptable. During the pre-melting phase, the heat rejection and heat storage were 54.55% and 45.45%, respectively.

Recently, the integration of nanoparticles, metal foams, and pin-fins with PCM were reported by different researchers under constant charging and discharging operations. Praveen et al. [36] conducted an experimental study to study the heat transfer performance of microencapsulated PCM (MEPCM) based graphene nano-platelets and paraffin in a finned heat sink. The authors found the charging durations of PCM and MEPCM of around 70 and 90 mins, respectively. However, there was no complete discharging achieved till at 180 mins for both PCM and MEPCM. Arshad et al. [37, 38] conducted a numerical study to investigate the combine effect of metal-foam, nanoparticles and PCM. The detailed natural convection heat transfer and melting phenomenon of Cu nanoparticles of different volume fraction of 1%, 3% and 5% dispersed into PCM were studied. A heat transfer enhancement of 2.86%, 2.19% and 1.63% with 1%, 3% and 5% volume fraction of Cu nanoparticles, respectively. Further, the authors found that Cu metal-foam and fully filled heat sink with PCM showed the better heat transfer rate. The Cu nanoparticles of 1% volume fraction exhibited the optimum volume fraction in comparison with 3% and 5% with metal-foam and PCM. A lower melting time reduction of 18.10% and higher rate of heat transfer of 8.12% were obtained with 1% Cu nanoparticles. Hassan et al. [39] used the graphene nanoplatelets (GNPs) and magnesium oxide (MgO) nanoparticles with PT-58, used as a PCM to develop the cPCM, and filled into copper foam having a porosity of 97%. It was concluded that GNPs/PCM based nano-PCM effectively reduced heat sink base temperature. The maximum reduction was obtained of 16% and 13.1% in case of GNPs/PCM/copper-foam and MgO/PCM/copper-foam, respectively at 0.02 wt.% nanoparticles loading and 1.54 kW/m^2 input heat flux. The authors reported that charging phase of PCM and nano-PCM completed after 90 mins, whereas there was no complete solidification occurred even after 100 mins. Fayyaz et al. [40] used the multi-walled carbon nanotubes (MWCNTs) as nanoparticles and dispersed in RT-42, used as a PCM, and filled in circular, square, and triangular-shaped pin-fin heat sinks. The results revealed that circular pin-fin heat sink showed the best thermal performance with based temperature reduction of 20.40% and 25.83% at 3 wt% and 6 wt% of MWCNTs in PCM, respectively. The charging phase duration was reported at 167 mins, whereas the discharging phase duration was longer than 250 mins. Zahid et al. [41] worked on the analysis of thermal behavior on different heat fluxes using square pin-fin, metal-fam and empty heat sink with Al_2O_3 and RT-54HC. They concluded that there was a significant drop in base temperature with increase in mass fraction of Al_2O_3 nanoparticles with Cu metal-foam heat sink. At input heat fluxes, the maximum enhancement in the working time of Cu metal-foam heat sink against 0.25 wt.% of NPs was 288%, 223.81%, and 202.56%, respectively.

A clear reflection from previous literature can be revealed that authors only conducted the passive cooling scheme by using fins, extended surfaces, porous medium, and nanomaterials either separately or collectively. To the best of the author's knowledge, no single study has been reported which explores the effects of fins, hybrid nanoparticles and external forced convection, cumulatively. In the current study, a combination of active and passive cooling technologies is presented by combing the air-cooled and PCM-cooled thermal management systems, as shown in Fig. 1. A numerical study is presented to combine air, nanoparticles, fins and PCM under natural and forced convection operating conditions to study the conventional air cooling and novel hybrid composite PCMs (HcPCMs) cooling techniques under constant heating loads. In addition, this study explores a combined effect of active-passive novel cooling technology based on the idea of latent heat thermal energy storage system for the efficient cooling of electronic devices.

2. Theoretical Methodology

2.1. Problem description

A conventional finned heat sink is used in the current study, adopted for the cooling of electronic components, and three different cases: (i) air-cooled, (ii) HcPCM-cooled, and (iii) hybrid (air-HcPCM) cooled finned heat sinks, as shown in Figure 2, are investigated numerically to explore the effect of natural and forced convection heat transfer performance at constant heating. A heat sink made of aluminium and a constant volume fraction of fins is chosen having high thermal conductivity and is lighter in weight. The hybrid nanoparticles of carbon additives, graphene oxide (GO), and multi-walled carbon nanotubes (MWCNTs) are selected because of their higher thermal conductivity and also these nanoparticles belong to carbon family as the selected PCM, RT-35HC, which makes a more stable and uniform mixture of cPCMs practically compared to the metallic or metallic-oxide nanoparticles with paraffin based PCMs [18]. The volume fraction (φ) of graphene oxide (GO) and multi-walled carbon nanotubes (MWCNTs) are chosen of 0%, 2%, 4%, and 6%. The heat flux (q) is varied from 25, 30, 35, and 40 kW/m^2 at the base of the heat sink. The thermophysical properties of aluminium, RT-35HC, GO and MWCNTs are provided in Table 1. The overall dimensions of the heat sink are $70 \times 70 \times 25$ mm^3 with walls and fin thickness of 5 and 2 mm, respectively, and the base of 5 mm where the constant heat flux is provided. Figure 3 shows the physical domain used with all boundary constraints to achieve the core objective of the current study.

Table 1: Thermophysical properties of RT-35HC, Aluminum, GO and MWCNTs [42, 43].

Property	**RT-35HC**	**Aluminum**	**GO**	**MWCNTs**
T_m (K)	308.15	-	-	-
T_l (K)	309.5	-	-	-
T_s (K)	306.5	-	-	-
L (J/kg)	240,000	-	-	-
ρ (kg/m^3)	825	2719	1800	2100
c_p (J/kg.K)	2000	871	717	630
k (W/m.K)	0.2	202.37	5000	3000
β (1/K)	0.0006	-	-	-
μ (Pa.s)	0.0235	-	-	-

2.2. Mathematical modeling

The conjugate heat transfer is considered to model the current phase-change heat transfer inside the heat sink between the PCM and hybrid nanoparticles. The heat transfer purely conduction through the finned heat sink. The thermophysical properties of the heat sink, HcPCM and nanoparticles remained constant. The liquid HcPCM is assumed as laminar, transient, and incompressible. The melting/solidification phenomenon of HcPCM is modeled as enthalpy-porosity formulation. The following governing equations are used to solve the continuity, momentum, and energy equations for the proposed problem [44, 45]:

Continuity:

$$\nabla.\overrightarrow{V} = 0 \tag{1}$$

Momentum:

$$\rho_{hcpcm}\frac{D\overrightarrow{V}}{Dt} = -\nabla p + \mu_{hcpcm}\nabla^2\overrightarrow{V} + \overrightarrow{S} + \overrightarrow{F_b} \tag{2}$$

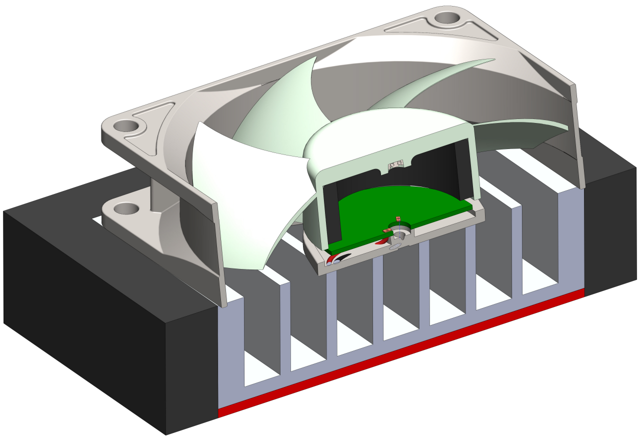

(a)

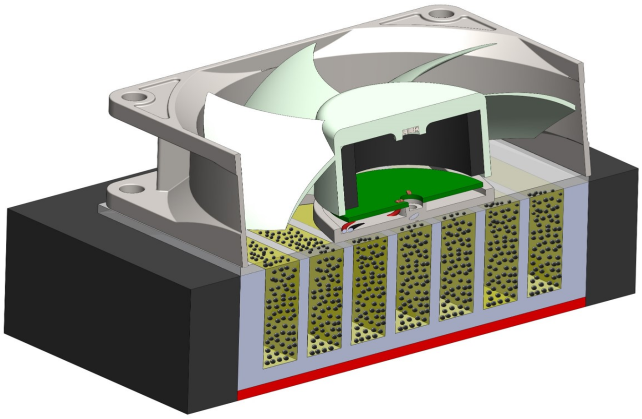

(b)

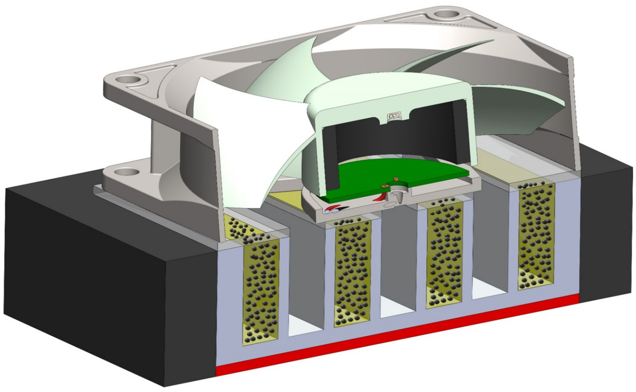

(c)

Figure 2: *An isometric cross–sectional view of (a) air-cooled finned heat sink, (b) HcPCM cooled finned heat sink and (c) hybrid (air-HcPCM) finned heat sink assembly.*

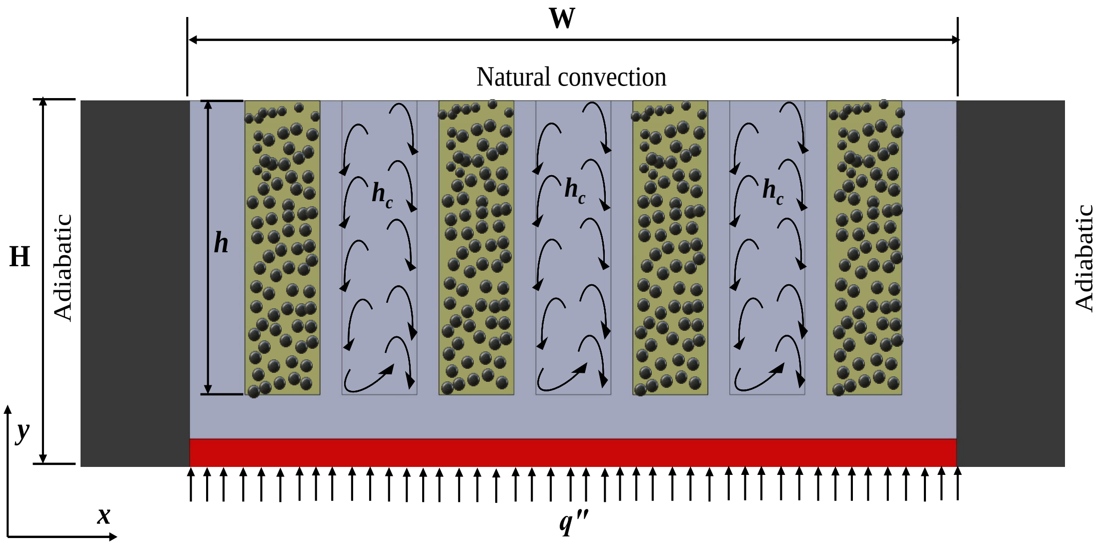

Figure 3: *Schematic diagram of the physical domain.*

Energy:

$$(\rho c_p)_{hcpcm}\frac{DT}{Dt} = \nabla.(k_{hcpcm}\nabla T) \tag{3}$$

Here, ρ_{hcpcm} is the density, t is the time, p is the pressure, μ_{hcpcm} is the dynamic viscosity, $(\rho c_p)_{hcpcm}$ is the thermal capacitance and k_{hcpcm} is the thermal conductivity of HcPCM. The $\overrightarrow{S}$ is Darcy's momentum mentioned in Equation 2, which can be defined as follows:

$$\overrightarrow{S} = -A_{mush}\frac{(1-l_f)^2}{l_f^3 - \varepsilon}.\overrightarrow{V} \tag{4}$$

Where, A_{mush} is a constant number (10^5) that illustrates the morphology of the mushy zone [46] and $\varepsilon = 0.001$ is only a constant value applied to avoid dividing by zero. Moreover, l_f is the liquid fraction of the PCM in the mushy region, and can be defined as:

$$l_f = \begin{cases} 0 & \text{if } T < T_s \\ \frac{T-T_s}{T_l-T_s} & \text{if } T_s < T < T_l \\ 1 & \text{if } T > T_l \end{cases} \tag{5}$$

The $\overrightarrow{F_b}$ in Equation 2 is the body force which is defined as follows:

$$\overrightarrow{F_b} = F_{bx}\vec{i} + F_{by}\vec{j} \tag{6}$$

Here,

$$F_{bx} = 0 \qquad\qquad F_{by} = -\rho_{ref} g\beta(T - T_{ref}) \tag{7}$$

Where, g is the gravitational body acceleration, T_{ref} is the reference temperature, and β is the thermal expansion coefficient has a value of $\beta = 0.0006\ K^{-1}$ [47, 48]. The term $-\rho_{ref} g\beta(T - T_{ref})$ is the Boussinesq approximation.

The specific heat ($c_{p_{hcpcm}}$) of HcPCM in Equation 3 can be defined as follow:

$$c_{p_{hcpcm}} = \begin{cases} c_{p_{hcpcm_s}} & \text{if } T < T_s \\ c_{p_{eff}} = c_{p_{hcpcm_s}}(1 - l_f) + c_{p_{hcpcm_l}}(l_f) + \frac{\Delta H_{hcpcm}}{T_l - T_s} & \text{if } T_s < T < T_l \\ c_{p_{hcpcm_l}} & \text{if } T > T_l \end{cases} \tag{8}$$

Here, $c_{p_{hcpcm_s}}$, $c_{p_{hcpcm_l}}$, T, T_s, T_l, and ΔH_{hcpcm} are the solid specific heat, liquid specific heat, average temperature, solidus temperature, and liquids temperature, and fractional latent–heat of the HcPCM, respectively.

The addition of hybrid carbon additives (GO+MWCNTs) into the PCM (RT-35HC) vary its thermophysical properties as the volume fraction of GO+MWCNTs is increased from 0% to 6%. The effective properties such as density (ρ_{hcpcm}), specific heat capacity ($c_{p_{hcpcm}}$), latent–heat of fusion (L_{hcpcm}), thermal expansion coefficient (β_{hcpcm}), dynamics viscosity (μ_{hcpcm}), and thermal conductivity (k_{hcpcm}) of HcPCMs are calculated using theoretical models of mixtures as follows [43, 49]:

$$\rho_{hcpcm} = \varphi_2\rho_{np_2} + \left[(1 - \varphi_2)\left\{\varphi_1\rho_{np_1} + (1 - \varphi_1)\rho_{pcm}\right\}\right] \tag{9}$$

$$(\rho c_p)_{hcpcm} = \varphi_2(\rho c_p)_{np_2} + \left[(1 - \varphi_2)\left\{\varphi_1(\rho c_p)_{np_1} + (1 - \varphi_1)(\rho c_p)_{pcm}\right\}\right] \tag{10}$$

$$(\rho L)_{hcpcm} = (1 - \varphi_1)(1 - \varphi_2)(\rho L)_{pcm} \tag{11}$$

$$(\rho\beta)_{hcpcm} = \varphi_2(\rho\beta)_{np_2} + \left[(1 - \varphi_2)\left\{\varphi_1(\rho c_p)_{np_1} + (1 - \varphi_1)(\rho\beta)_{pcm}\right\}\right] \tag{12}$$

$$\mu_{hcpcm} = \frac{\mu_{pcm}}{(1 - \varphi_1)^{2.5}(1 - \varphi_2)^{2.5}} \tag{13}$$

$$\frac{k_{hcpcm}}{k_{cpcm}} = \frac{k_{np_2} + (sf-1)k_{cpcm} - (sf-1)(k_{cpcm} - k_{np_2})\varphi_2}{k_{np_2} + (sf-1)k_{cpcm} + (k_{cpcm} - k_{np_2})\varphi_2} \tag{14}$$

where:

$$\frac{k_{cpcm}}{k_{pcm}} = \frac{k_{np_1} + (sf-1)k_{pcm} - (sf-1)(k_{pcm} - k_{np_1})\varphi_1}{k_{np_1} + (sf-1)k_{pcm} + (k_{pcm} - k_{np_1})\varphi_1} \tag{15}$$

In above Equations 9–15, φ_1 and φ_2 represent the volume fractions of nanoparticles of type 1 and nanoparticles of type 2, respectively. The subscripts *hcpcm*, *np*, *pcm*, np_1 and np_2 refer to the HcPCM, nanoparticles, PCM, nanoparticles of type 1 and nanoparticles of type 2, respectively.

2.3. Mesh independency

The grid independence test has been conducted to find the optimum mesh size of the heat sink to avoid the effects of numerical accuracy and to reduce the computational cost. The four different mesh categories such as normal, fine, finer, and extra finer of element sizes of 4643, 6636, 10111 and 19004, respectively, of a PCM-cooled heat sink to consider the effects of both air and PCM, cumulatively. The results of average heat sink temperature and liquid fraction for selected meshes sizes are presented in Figures 4a and 4b, respectively. From Figure 4, it can be seen that there is no significant difference between normal to extra finer meshes in average heat sink temperature and liquid fraction. This is because of the low PCM upfront velocity and thermal front movement which reflects a low Peclet number and Courant number situation. Since, the deviation between extra finer and finer mesh sizes is minimum, thus the finer mesh with element size 10111 is chosen for further simulation in current study. In similar pattern, the optimum mesh size is considered for air-cooled and hybrid cooled finned heat sinks.

2.4. Numerical method and validation

The governing equations Eqs. 1–8 are solved using a finite element method (FEM) based computational tool, COMSOL Multiphysics. The problem is computed for a linear set of equations with Parallel Direct Sparse Solver Interface (PARDISO) in fully-coupled automated preordering algorithm mode. Implicit backward differentiation formula (BDF) is used for time-stepping with automatic step size selection between BDF order 1-2. The tolerance termination technique is adapted where custom relative tolerance value 10^{-4} is used for all outcome variables. A backward Euler method with 10^{-3} fraction for initial step is used for consistent initialization of the algebraic variables.

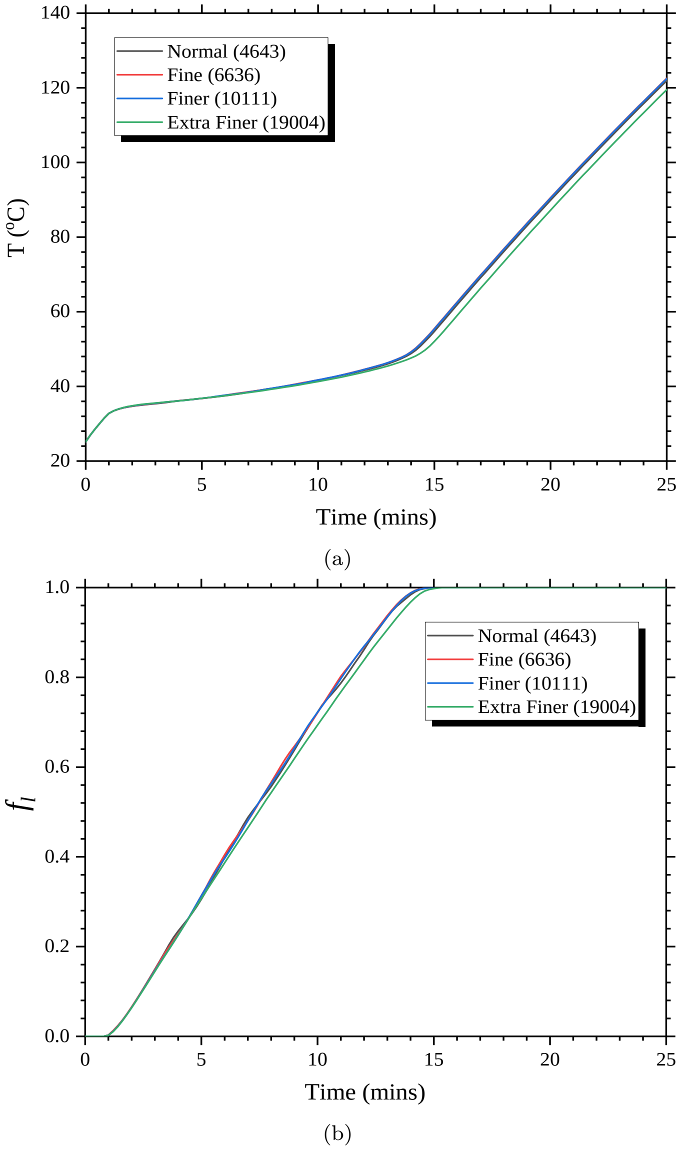

Figure 4: *Mesh independence results of (a) average heat sink temperature (b) liquid fraction with time, for different meshes.*

The present results of liquid fraction, to validate the current developed governing model, are validated a comparison to the results of with Sunku Prasad et al. [44]. Figure 5 presents the results of f_l against the time at power level of 12 W and RT-35HC is used as PCM, filled in a plate-fin heat sink. A good agreement can be seen between current numerical and reported results of PCM melting process. The present results of f_l is validated with experimental results of the PCM (lauric acid) and fin combination reported by Kamkari and Shokouhmand [48], as shown in Fig. 6. A rectangular domain with 3 fins at 90° is considered with an interior of 50 mm in width, 120 mm in height and 120 mm in depth. An input wall temperature of 70 °C is applied and the results of the melting processes are compared. A good agreement is obtained between the numerical and experiment results

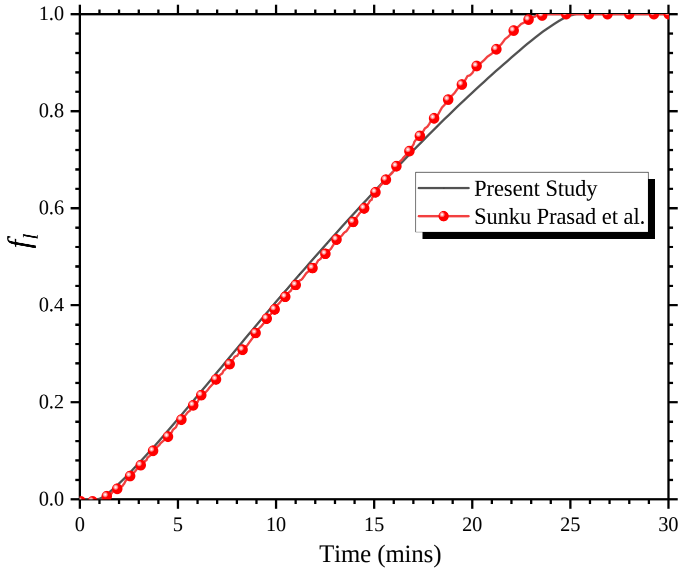

Figure 5: *Validation of present numerical results of the liquid fraction compared with Sunku Prasad, et al. [44].*

of lauric acid f_l. The variations in results may be due to radiation and conduction heat transfer and PCM properties varying in experimentation with temperature and time.

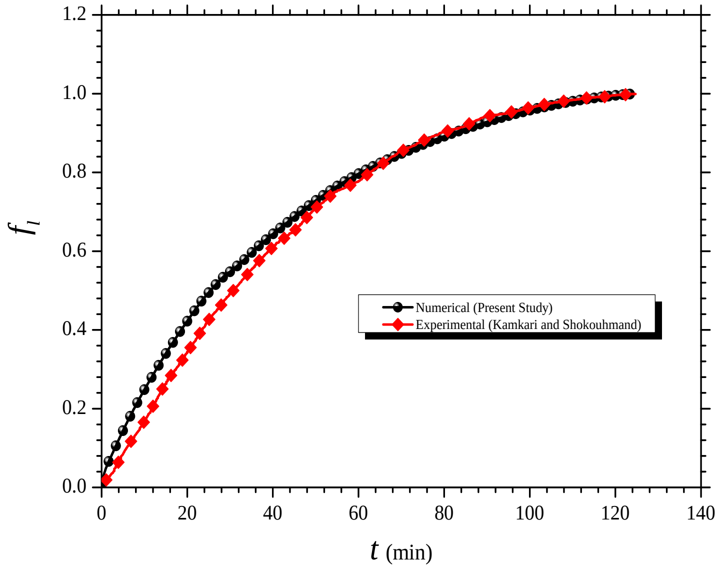

Figure 6: *Validation of present numerical results with experimental results by Kamkari and Shokouhmand [48].*

3. Results and discussion

3.1. Performance of air-cooled finned heat sink

The cooling performance of an air-cooled finned heat sink is presented in Figure 7 by varying the different heat fluxes (q) and convective heat transfer coefficient (h_c). The values of q are varied as 25, 30, 35, and 40 kW/m^2 as shown in Figures 7a, 7b, 7c, and 7d, respectively, at different h_c of 10, 20, 30, 40, 50, and 100 W/m^2.K. As expected, the effect of h_c for each heat flux clearly shows that the increasing h_c reduces the overall temperature of the heat sink. This shows that the effects of forced convection heat transfer mode ($h_c > 10$) are more predominant on the cooling performance of the heat sink compared with the natural convective heat transfer mode ($h_c \leq 10$). During the natural convective heat transfer, the heat sink cools or dissipates the excessive heat generated by the electronic components under natural convection effects i.e. without the effect of external force and air motion is caused by buoyancy. As a result of this, the temperature of the heat sink rises dramatically initially and remains constant around 15 min till the end. Whereas, during the forced convective heat transfer, in case of $h_c > 10$, the heat sink transfers the internal heat due to the effect of external forced flow of air. Thus, the external flow of air flowing through the heat sink fins reduce the heat sink base temperature that can be clearly seen in all cases presented in Figures 7a-7d as the h_c varies from 10 to 100 W/m^2.K. Furthermore, it can be revealed from Figures 7a-7d that the lowest heat sink temperature is obtained in case of $h_c = 100$ W/m^2.K which is as expected. However, it also reveals clearly that at $h_c = 40$ and $h_c = 50$ W/m^2.K, the heat sink temperature lies between $\approx 30 - 40^o$C, which is the optimum average body temperature range for a human [50]. The effect of temperature distribution at different heat fluxes of q 25, 30, 35, and 40 kW/m^2 under natural convection heat transfer coefficient ($h_c = 10$ W/m^2.K) is shown in Figure 7e. Temperature distribution clearly shows that with the increase of q the heat sink temperature increases, as expected. There is a sharp increase in the heat sink temperature initially because of higher heat capacity. However, it reaches a contact level because of thermal inertia, since at this point, the heat sink stores the heat rather than to transfer it.

3.2. Performance of HcPCM-cooled finned heat sink

The temperature variations at different volume fractions ($\varphi = 0\%$, 2%, 4%, and 6%) of hybrid nanoparticles (GO+MWCNTs), different h_c of 10, 20, 30, 40, 50, and 100 W/m^2.K and $q = 40$ kW/m^2 are shown in Figure 8a-8d. Two major significances occurred during the melting of HcPCM inside the finned heat sink as the h_c is applied at the top surface of the heat sink. Firstly, it can be seen clearly that with the increase of h_c the heat sink temperature decreases and minimum temperature is achieved at $h_c = 100$ W/m^2.K, as expected. Secondly, the latent heating phase is also increased as the h_c increases from 10 to 100 W/m^2.K. This is because of higher heat transfer from the heat sink base towards the

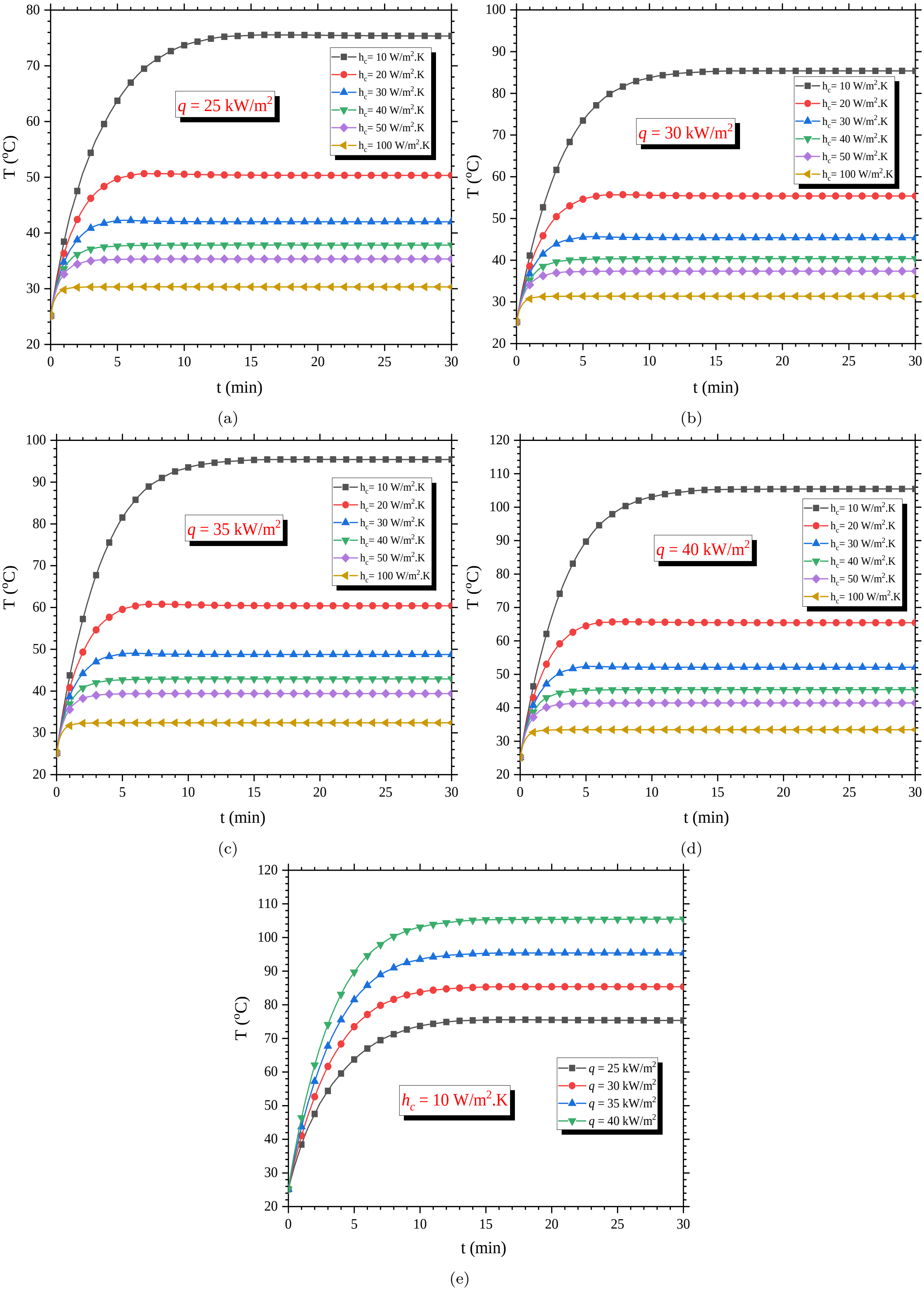

Figure 7: *Temperature-Time variations of air-cooled finned heat sink under various* q *and* h_c*: (a)* $q = 25$ kW/m^2*, (b)* $q = 30$ kW/m^2*, (c)* $q = 35$ kW/m^2*, (d)* $q = 40$ kW/m^2 *and (e)* $h_c = 10$ $W/m^2.K$*.*

ambient due to the effect of forced convective heat transfer coefficient ($h_c > 10$ W/m^2.K) compared to the natural convective heat transfer coefficient ($h_c \leq 10$ W/m^2.K). The melt fraction (l_f) distribution of HcPCM based finned heat sink of hybrid nanoparticles dispersion at different $\varphi =$ is presented in Figure 9 under natural and forced heat transfer heating environments. It can be seen from Figures 9a-9d that in all cases of φ, l_f is decreased with the increase of h_c from natural to forced convection heat transfer conditions. This shows that the melting time (t_m) of HcPCM is enhanced resulting in extended the latent heating phase duration. There is no significant variation in l_f during before and after sensible heating mode, however, the HcPCM melting variation becomes significance while the HcPCM reaches the phase of complete melting. The effect of forced convection heat transfer mode shows that melting of the HcPCM is delayed and increases the heat transfer rate resulting in it reducing the heat sink base temperature. The comparison of all cases of $\varphi = 0\%$, 2%, 4%, and 6% at $h_c = 10$ W/m^2.K and constant heating is presented in Figure 10a and 10b for heat sink base temperature and melting performance, respectively. From Figure 10a, it can be revealed that the addition of GO+MWCNTs hybrid nanoparticles reduces the heat sink base temperature. Although, that reduction in heat sink temperature is not so significant, however, nanoparticles enhanced the temperature distribution and uniformity of HcPCM melting. Furthermore, it can also be seen that as the φ is increased from 0% to 6% the latent heating phase is shortened and heat sink base temperature is increased during the post-sensible melting phase. The comparison of φ represented in Figure 10b shows that l_f is increased as the φ increases from 0% to 6% resulting in a reduction of the t_m of HcPCM.

3.3. Performance of hybrid HcPCM cooled finned heat sink

The cooling performance of a hybrid (air-HcPCM) finned heat sink (as shown in Figure 2c) operating under different h_c and φ at constant heating of $q = 40$ kW/m^2 is presented in Figure 11. A clear evidence can be seen that the thermal performance of a hybrid heat sink integrated with HcPCM and forced flow through the fins immensely is improved in terms of reduction of the heat sink base temperature. A clear difference in the drop of heat sink temperature can be seen in each case shown in Figures 11a-11d due the effect of h_c. In addition to this, there is less or no significant phase change effect observed at $h_c = 100$ W/m^2.K of HcPCM which means the amount of heat energy that the hybrid heat sink is absorbing from the electronic component is releasing approximately equal to that amount of heat energy towards the ambient. This is eventually maintaining the heat sink base tem-

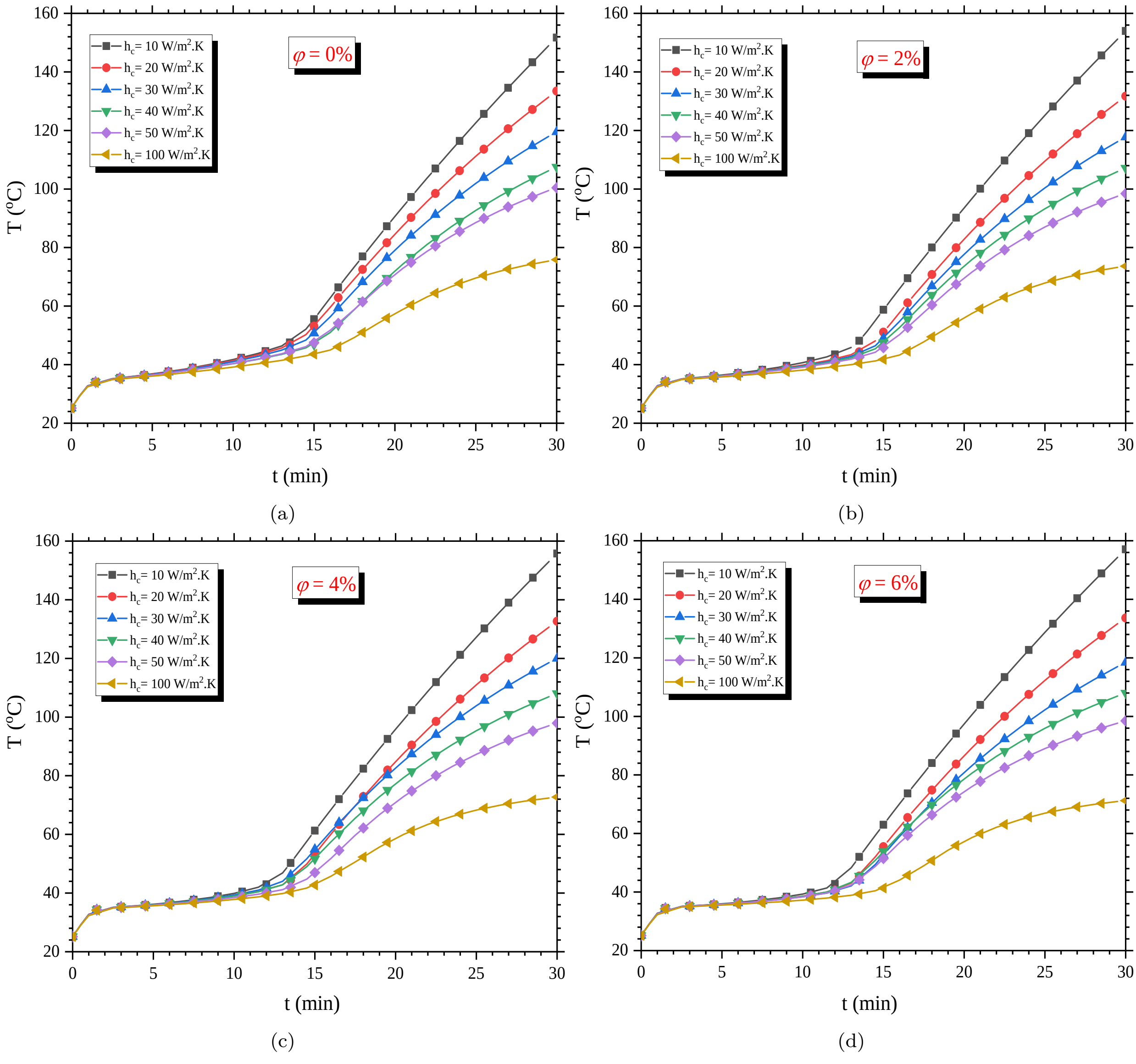

Figure 8: *Temperature-Time variations of HcPCM cooled finned heat sink under various* φ = *(a) 0%, (b) 2%, (c) 4%, and (d) 6%.*

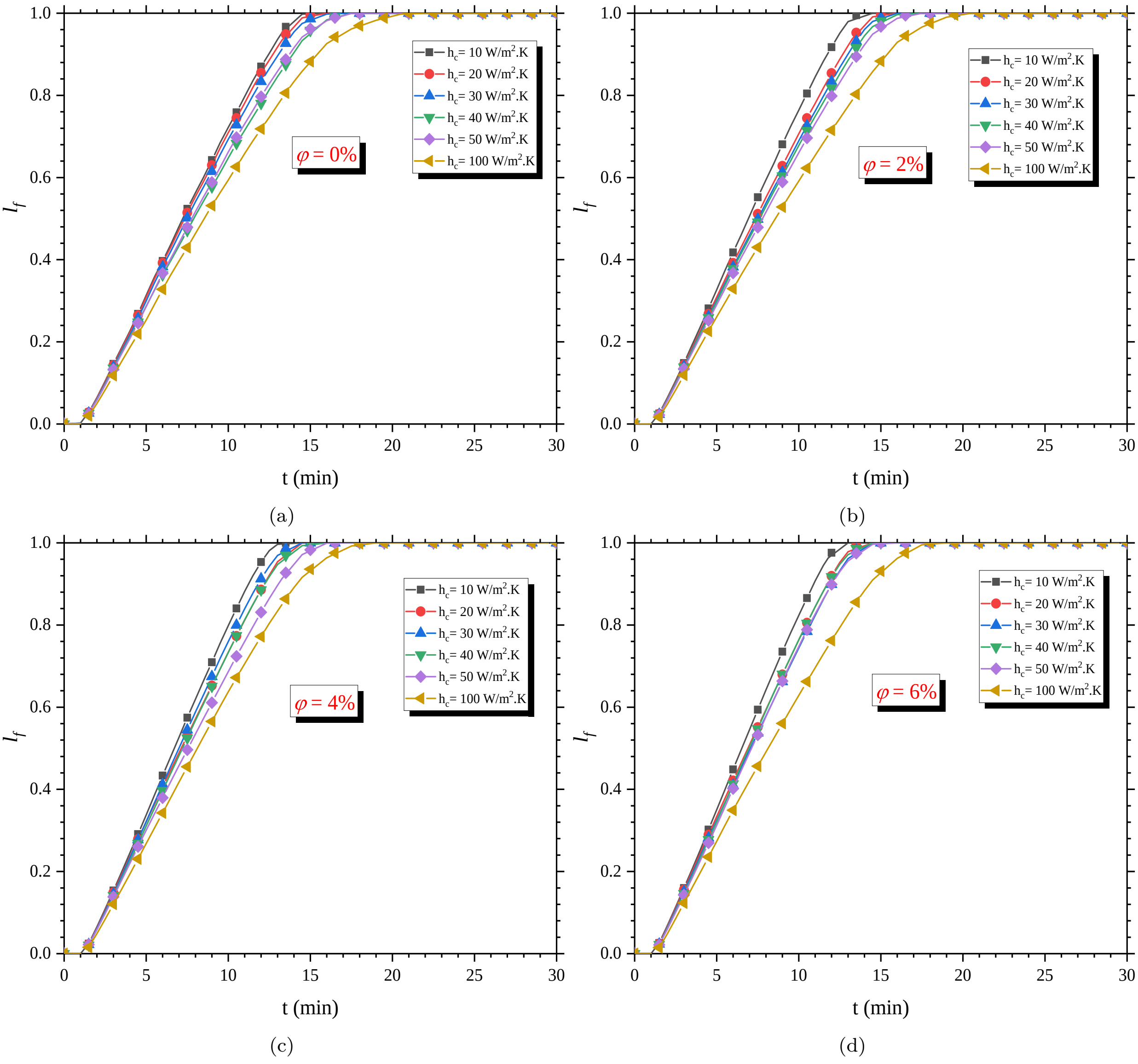

Figure 9: *The l_f variations of HcPCM cooled finned heat sink under various φ = (a) 0%, (b) 2%, (c) 4%, and (d) 6%.*

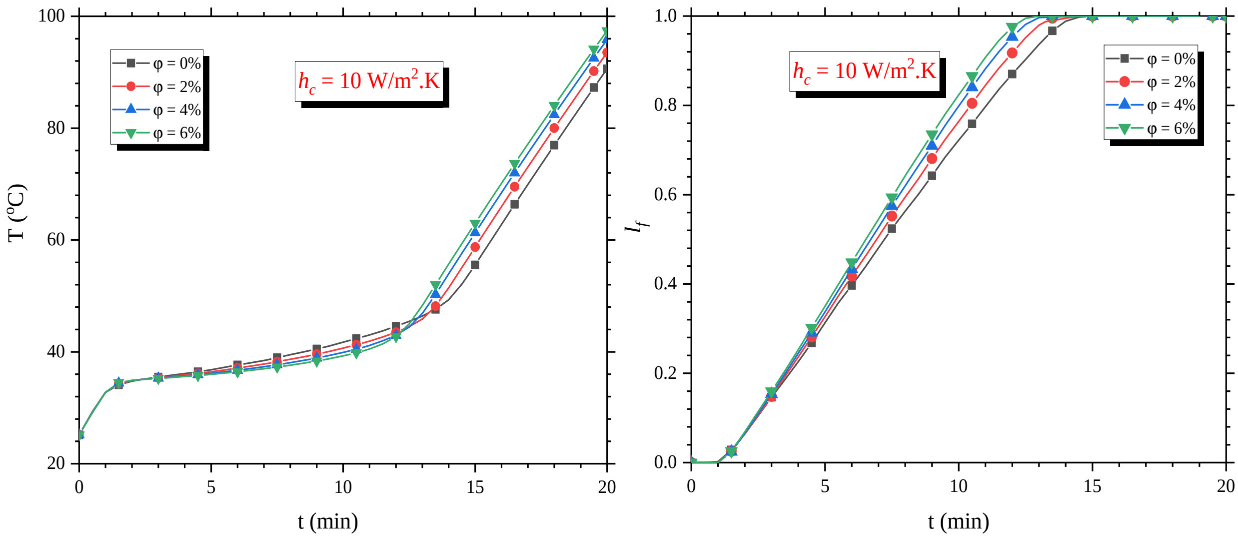

(a) (b)

Figure 10: *(a) Time histories and (b) l_f of HcPCM cooled finned heat sink temperature under various $\varphi =$ at $h_c = 10\ W/m^2.K$.*

perature within a safe operating limit and provides the highest cooling performance. The latent heating phase of HcPCM filled in finned heat sink is extended with the increase of h_c due to a higher heat transfer rate at each φ. At $\varphi = 0\%$, the slight change in the latent heating phase around 26 mins which is showing the starting of a post-sensible heating phase. However, at $\varphi = 2\%$, 4%, and 6% , there is no post-sensible heating phase is revealed till 30 mins of operation and only latent heating phase continues. This shows the effect of forced convection heat transfer by applying an additional cooling media such as air in the present case shows the more efficient and higher thermal cooling enhancement. The melting distribution of HcPCM in hybrid heat sink in terms of l_f is presented in Figure 12 at different h_c and φ. It is shown in Figures 12a-12d that l_f is decreasing and t_m is increasing with the increase of h_c from 10 to 100 W/m^2.K. Furthermore, it is revealed that only in the case of $\varphi = 0\%$ l_f reaches to the value of 1, means HcPCM completely melts at $h_c = 100$ W/m^2.K. However, in case of $\varphi = 2\%$, 4%, and 6%, l_f does not reaches to $l_f = 1$ at $h_c = 100$ W/m^2.K which shows that there is no complete melting of HcPCM even after 30 min of heating.

The comparison of $\varphi = 0\%$, 2%, 4%, and 6% of heat sink temperature and l_f at $h_c = 10$ W/m^2.K is shown in Figures 13a and 13b, respectively. There is a slight variation in heat sink temperature observed at $\varphi = 2\%$, 4%, and 6% during latent heating and post-sensible phases, however, the heat sink temperature is lower than $\varphi = 0\%$ in all cases. Similarly, the l_f variations show that l_f increases with the increase of φ at $h_c = 10$ W/m^2.K. This shows that the latent heating phase duration or t_m is reduced with the addition of hybrid nanoparticles of GO+MWCNTs. The presence of hybrid nanoparticles into the pure PCM reveal no significance impact on the thermal performance. However, the addition of hybrid nanoparticles especially carbon-additives improve the thermal conductivity, specific heat capacity, reduce the latent heat capacity and enhance the uniformity while melting/solidification phase transformation [18, 51].

This isotherm and streamline contours of temperature distribution of hybrid finned heat sink integrated with HcPCM at $\varphi = 6\%$ are shown in Figure 14. The temperature distribution at different time steps of 3, 6, 9, and 12 mins are presented for h_c of 10, 20, 30, 40, 50, and 100 W/m^2.K. A dominant effect of conduction heat transfer can be seen at the initial stage of the heating. The higher temperature can be seen at the base of heat sink towards the top side and lower temperature distribution is revealed between the fins filled with HcPCM. The lower temperature is because of the absorption of heat by the HcPCM, supplied at the base of heat sink, because of its latent heat of fusion. Additionally, the lower temperature distribution can be seen on surface of fins subjected to the air flow through the fins. The additional force flow of air, which acts as a act cooling, further increase the heat transfer rate from the heat sink base and HPCM and fins network to towards the ambient. The melting phenomenon of hybrid HcPCM finned heat sink is presented in Figure 15 subjected of natural and forced convective heat transfer modes with h_c of 10, 20, 30, 40, 50, and 100 W/m^2.K. The hybrid nanoparticles of GO+MWCNTs of $\varphi = 6\%$ enhances the melting rate over time during constant heating, however, the external effect of airflow reduces the melting rate which can be seen from Figure 15a-15d at $h_c = 10$ W/m^2.K and Figures 15u-15x at $h_c = 100$ W/m^2.K. There is no complete melting of HcPCM at $h_c = 100$ W/m^2.K even at 12min of heating, whereas, HcPCM completely melts at 12min in case of $h_c = 10$, 20, 30, and 40 W/m^2.K.

The isotherm and streamline contours of hybrid HcPCM finned heat sink filled at different $\varphi = 0\%$, 2%, 4%, and 6% subject to natural effect of $h_c = 10$ W/m^2.K are shown in Figure 16 at various time periods. Similarly, the melt fraction contours of hybrid HcPCM finned heat sink filled at different $\varphi = 0\%$, 2%, 4%, and 6% subject to natural effect of $h_c = 10$ W/m^2.K are shown in Figure 17 at various periods. The isotherm and streamlines contours show the higher heat sink temperature at fins surfaces and lower temperature between the cPCM filled fins. Moreover, with the increase of heating duration e.g. 3, 6, 9, and 12 mins at a specific φ, the heat sink temperature increases and conduction heat transfer is the dominant to transfer the heat inside the heat sink. However, the convection heat transfer is the predominant mode to transfer the heat between the fins due to the external flow of air. Higher melt fraction of HcPCM is revealed with the increase of heating operation for each φ. Also, at a specific time period, with the increase of φ from 0% to 6%, the melt fraction is also increases at constant heating because of absorption of heat and showing the complete phase transformation process.

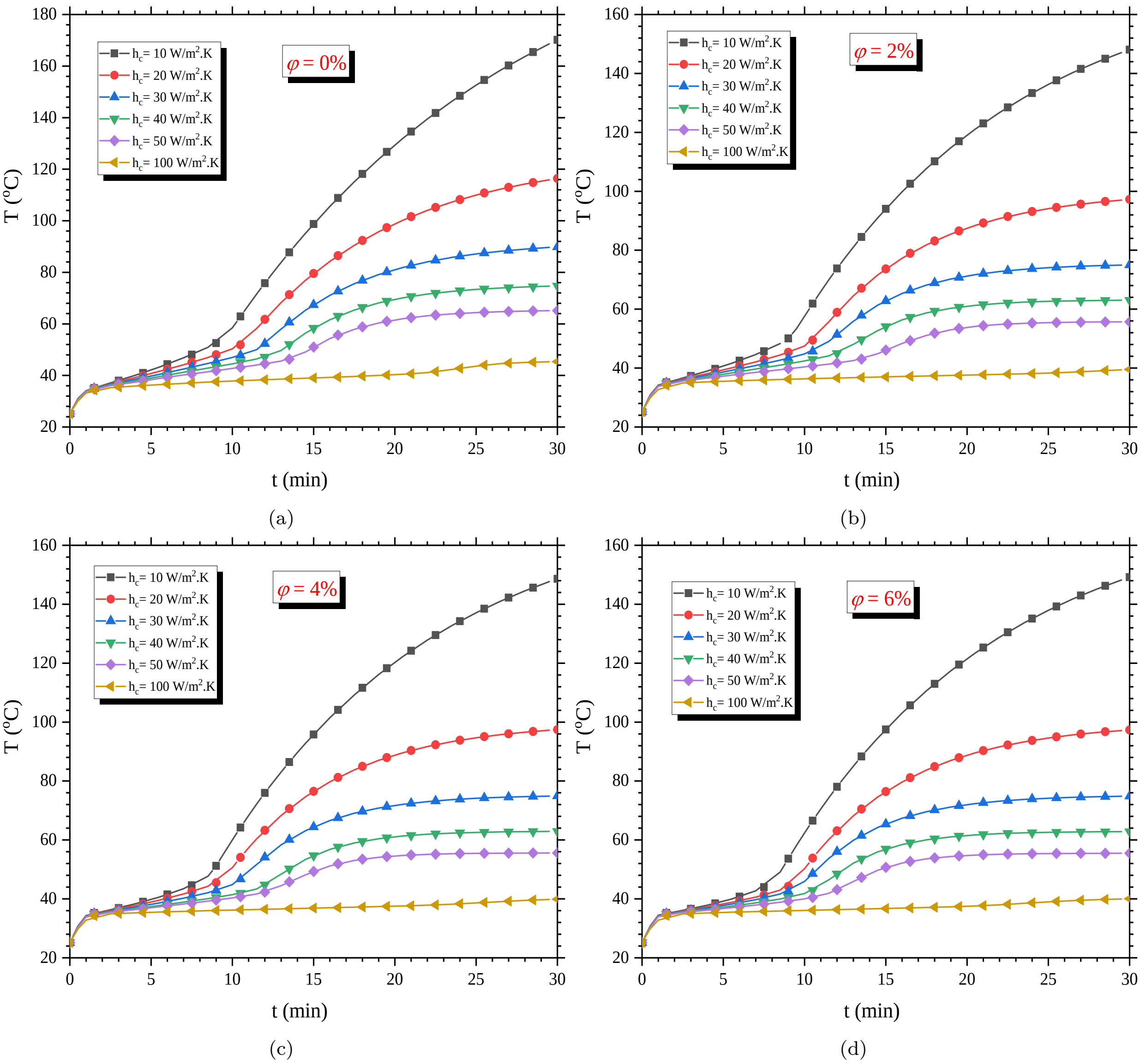

Figure 11: *Temperature-Time variations of hybrid HcPCM cooled finned heat sink under various* φ = *(a) 0%, (b) 2%, (c) 4%, and (d) 6%..*

4. Conclusion

A transient two-dimensional numerical study is carried out with the idea of to integrate the active and passive cooling method in a novel thermal management technology for lower to medium heat flux dissipating electronic devices. The current study presents conventional

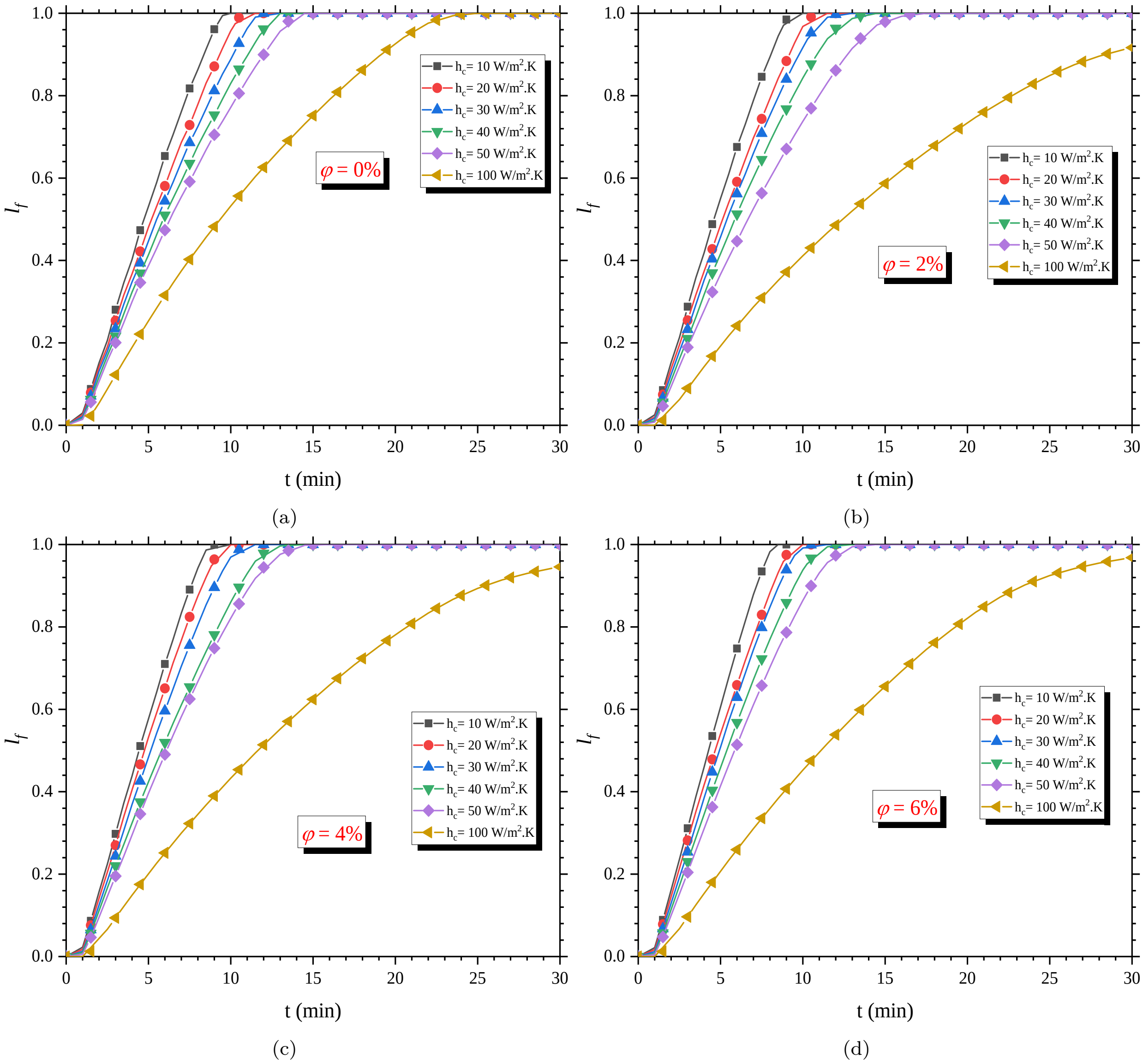

Figure 12: *The l_f variations of hybrid HcPCM cooled finned heat sink under various φ = (a) 0%, (b) 2%, (c) 4%, and (d) 6%*

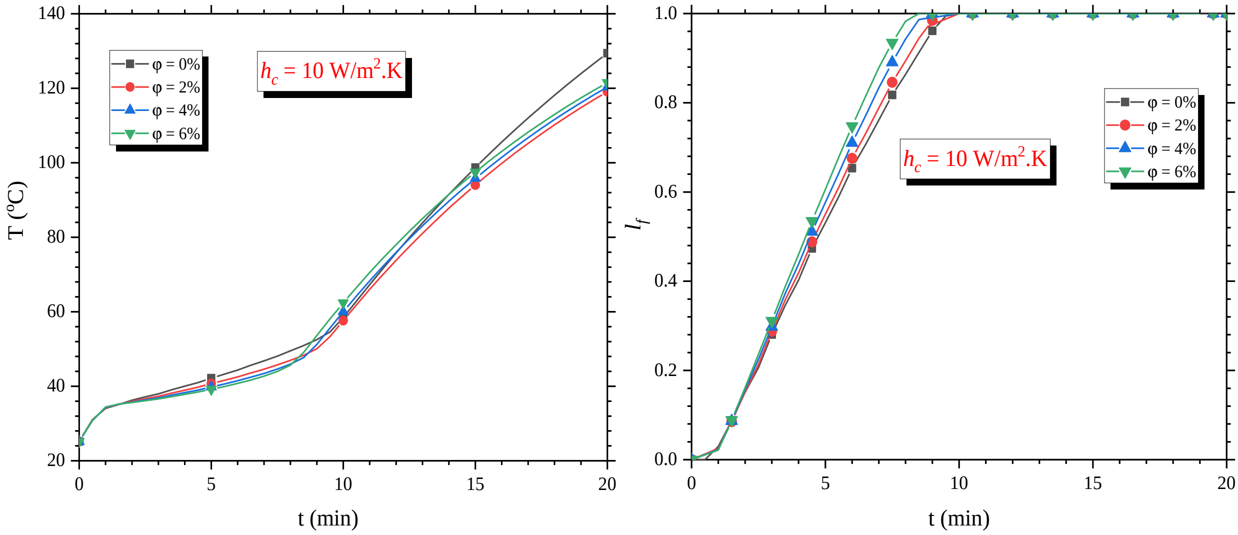

(a) (b)

Figure 13: *(a) Time histories and (b) l_f of hybrid HcPCM cooled finned heat sink temperature under various $\varphi =$ at $h_c = 10\ W/m^2.K$*

air cooling method as an active cooling method and PCM-based heat sink as a passive cooling method. The hybrid composite PCM (HcPCM) is designed by dispersing the hybrid nanoparticles of GO and MWCNTs with volume fractions of 0%, 2%, 4%, and 6% in RT-35HC. The convective heat transfer coefficient (h_c) is varied from $10 - 100\ \mathrm{W/m^2.K}$ and heat flux (q) is varied from 25, 30, 35, and 40 $\mathrm{kW/m^2}$. A plate-fin heat sink of constant volume fractions, made of aluminium, is selected and three different finned heat sinks such as air-cooled, HcPCM cooled and hybrid HcPCM cooled configurations are investigated numerically. The following main key outcomes are revealed in present study:

- The effect of $\mathrm{h}_c = 10\ \mathrm{W/m^2.K}$ on an air-cooled heat sink did not reduce the heat sink base temperature and a higher temperature rise is observed with the increase of q. However, when the h_c is between 30 to 50 $\mathrm{W/m^2.K}$, the base temperature reduces within the human comfortable temperature range at $q = 25\ \mathrm{kW/m^2}$.

- The HcPCM based finned heat sinks reveal that the addition of GO+MWCNTs in RT-35HC reduces the heat sink base temperature with increase of hybrid nanoparticles concentration from 0% to 6%. Meanwhile, the effect of h_c further reduces base temperature and keeps the heat sink in safe temperature operating limit. This shows that the combined effects of hybrid nanoparticles and h_c reduces the average heat sink temperature significantly and uniformed the melting process of PCM.

- In the case of a hybrid HcPCM finned heat sink, the h_c significantly improves the heat

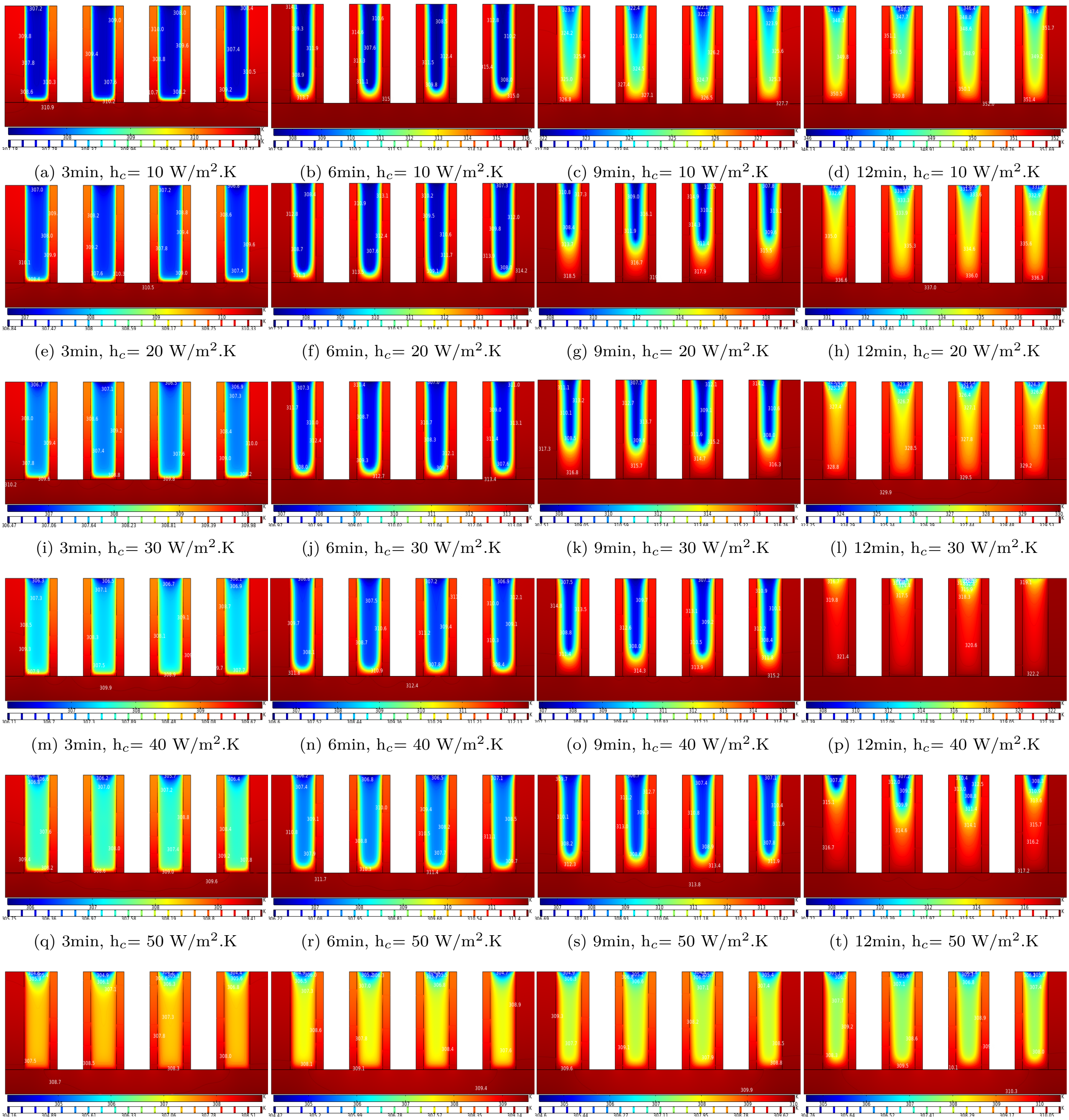

(a) 3min, h_c= 10 W/m^2.K (b) 6min, h_c= 10 W/m^2.K (c) 9min, h_c= 10 W/m^2.K (d) 12min, h_c= 10 W/m^2.K

(e) 3min, h_c= 20 W/m^2.K (f) 6min, h_c= 20 W/m^2.K (g) 9min, h_c= 20 W/m^2.K (h) 12min, h_c= 20 W/m^2.K

(i) 3min, h_c= 30 W/m^2.K (j) 6min, h_c= 30 W/m^2.K (k) 9min, h_c= 30 W/m^2.K (l) 12min, h_c= 30 W/m^2.K

(m) 3min, h_c= 40 W/m^2.K (n) 6min, h_c= 40 W/m^2.K (o) 9min, h_c= 40 W/m^2.K (p) 12min, h_c= 40 W/m^2.K

(q) 3min, h_c= 50 W/m^2.K (r) 6min, h_c= 50 W/m^2.K (s) 9min, h_c= 50 W/m^2.K (t) 12min, h_c= 50 W/m^2.K

(u) 3min, h_c= 100 W/m^2.K (v) 6min, h_c= 100 W/m^2.K (w) 9min, h_c= 100 W/m^2.K (x) 12min, h_c= 100 W/m^2.K

Figure 14: *Comparison of isotherms contours of hybrid HcPCM filled finned heat sink at φ = 6% and h_c = 10, 20, 30, 40, 50, and 100 W/m^2.K at various time-steps.*

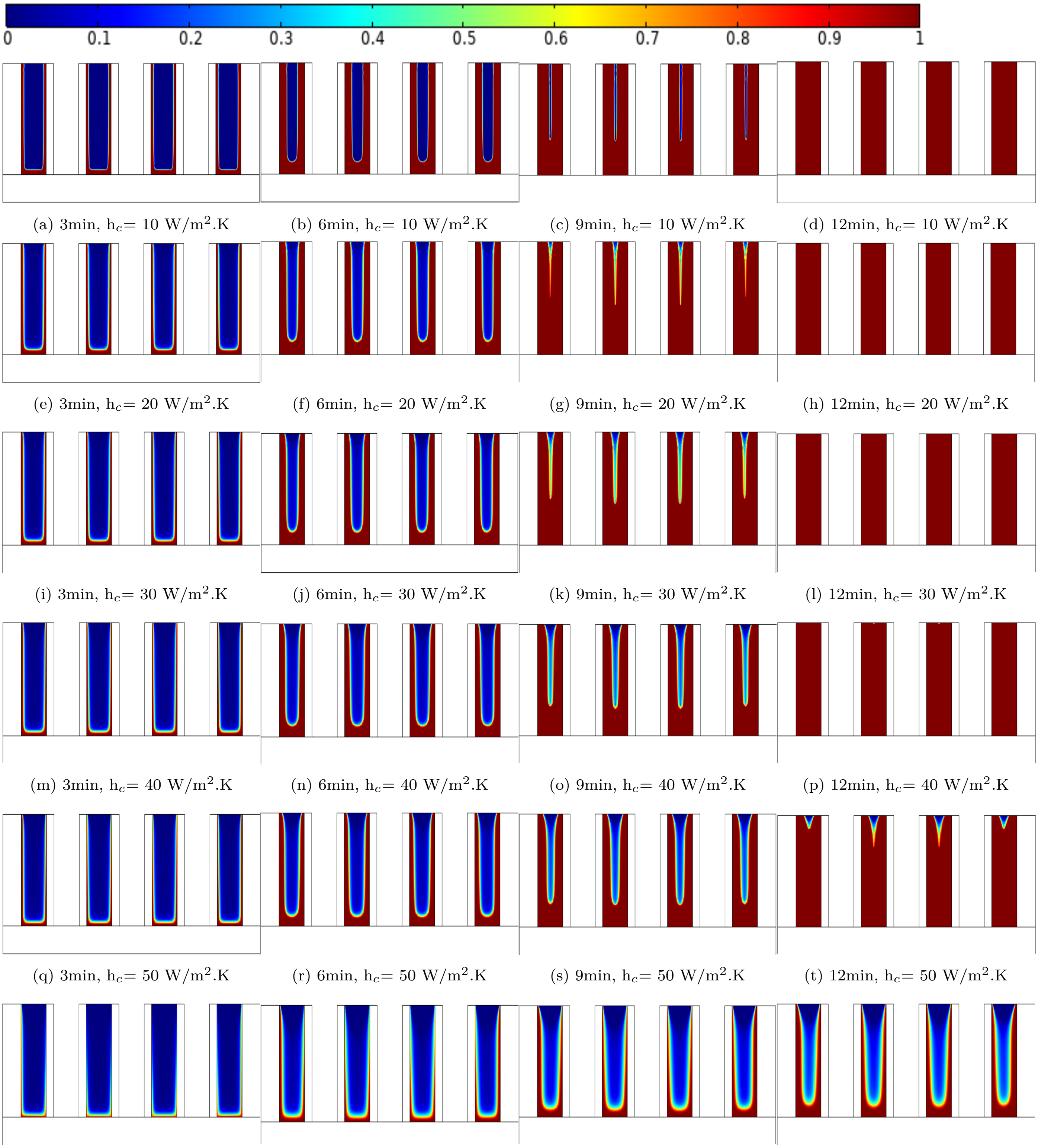

(a) 3min, h_c= 10 W/m^2.K (b) 6min, h_c= 10 W/m^2.K (c) 9min, h_c= 10 W/m^2.K (d) 12min, h_c= 10 W/m^2.K

(e) 3min, h_c= 20 W/m^2.K (f) 6min, h_c= 20 W/m^2.K (g) 9min, h_c= 20 W/m^2.K (h) 12min, h_c= 20 W/m^2.K

(i) 3min, h_c= 30 W/m^2.K (j) 6min, h_c= 30 W/m^2.K (k) 9min, h_c= 30 W/m^2.K (l) 12min, h_c= 30 W/m^2.K

(m) 3min, h_c= 40 W/m^2.K (n) 6min, h_c= 40 W/m^2.K (o) 9min, h_c= 40 W/m^2.K (p) 12min, h_c= 40 W/m^2.K

(q) 3min, h_c= 50 W/m^2.K (r) 6min, h_c= 50 W/m^2.K (s) 9min, h_c= 50 W/m^2.K (t) 12min, h_c= 50 W/m^2.K

(u) 3min, h_c= 100 W/m^2.K (v) 6min, h_c= 100 W/m^2.K (w) 9min, h_c= 100 W/m^2.K (x) 12min, h_c= 100 W/m^2.K

Figure 15: *Comparison of liquid fraction contours of hybrid HcPCM filled finned heat sink at* $\varphi = 6\%$ *and* h_c = *10, 20, 30, 40, 50, and 100 W/m^2.K at various time-steps.*

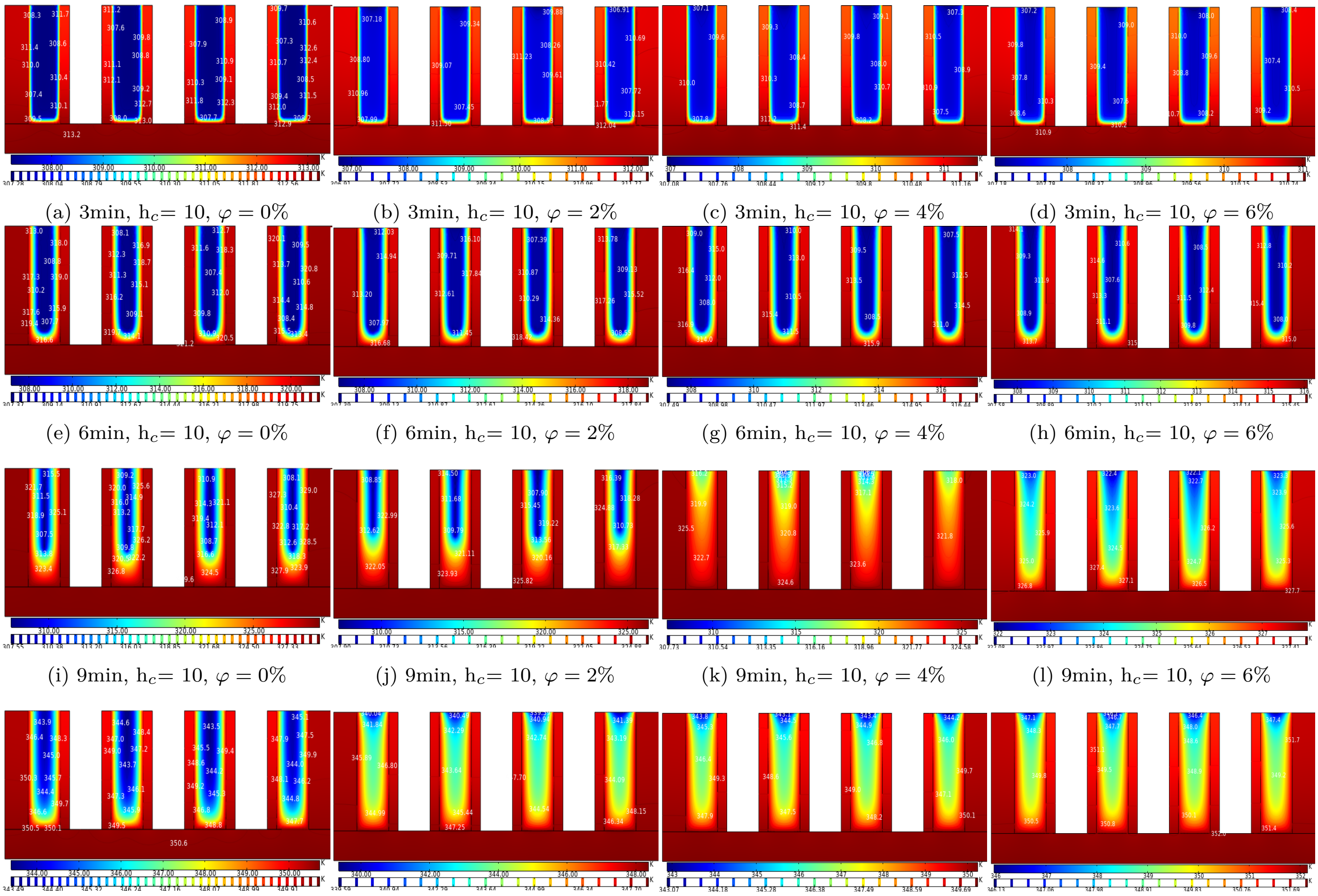

(a) 3min, h$_c$= 10, $\varphi = 0\%$ (b) 3min, h$_c$= 10, $\varphi = 2\%$ (c) 3min, h$_c$= 10, $\varphi = 4\%$ (d) 3min, h$_c$= 10, $\varphi = 6\%$

(e) 6min, h$_c$= 10, $\varphi = 0\%$ (f) 6min, h$_c$= 10, $\varphi = 2\%$ (g) 6min, h$_c$= 10, $\varphi = 4\%$ (h) 6min, h$_c$= 10, $\varphi = 6\%$

(i) 9min, h$_c$= 10, $\varphi = 0\%$ (j) 9min, h$_c$= 10, $\varphi = 2\%$ (k) 9min, h$_c$= 10, $\varphi = 4\%$ (l) 9min, h$_c$= 10, $\varphi = 6\%$

(m) 12min, h$_c$= 10, $\varphi = 0\%$ (n) 12min, h$_c$= 10, $\varphi = 2\%$ (o) 12min, h$_c$= 10, $\varphi = 4\%$ (p) 12min, h$_c$= 10, $\varphi = 6\%$

Figure 16: *Comparison of isotherms contours of hybrid HcPCM filled finned heat sink at $\varphi = 0\%, 2\%$, 4% and 6% and h_c = 10 W/m^2.K at various time-steps.*

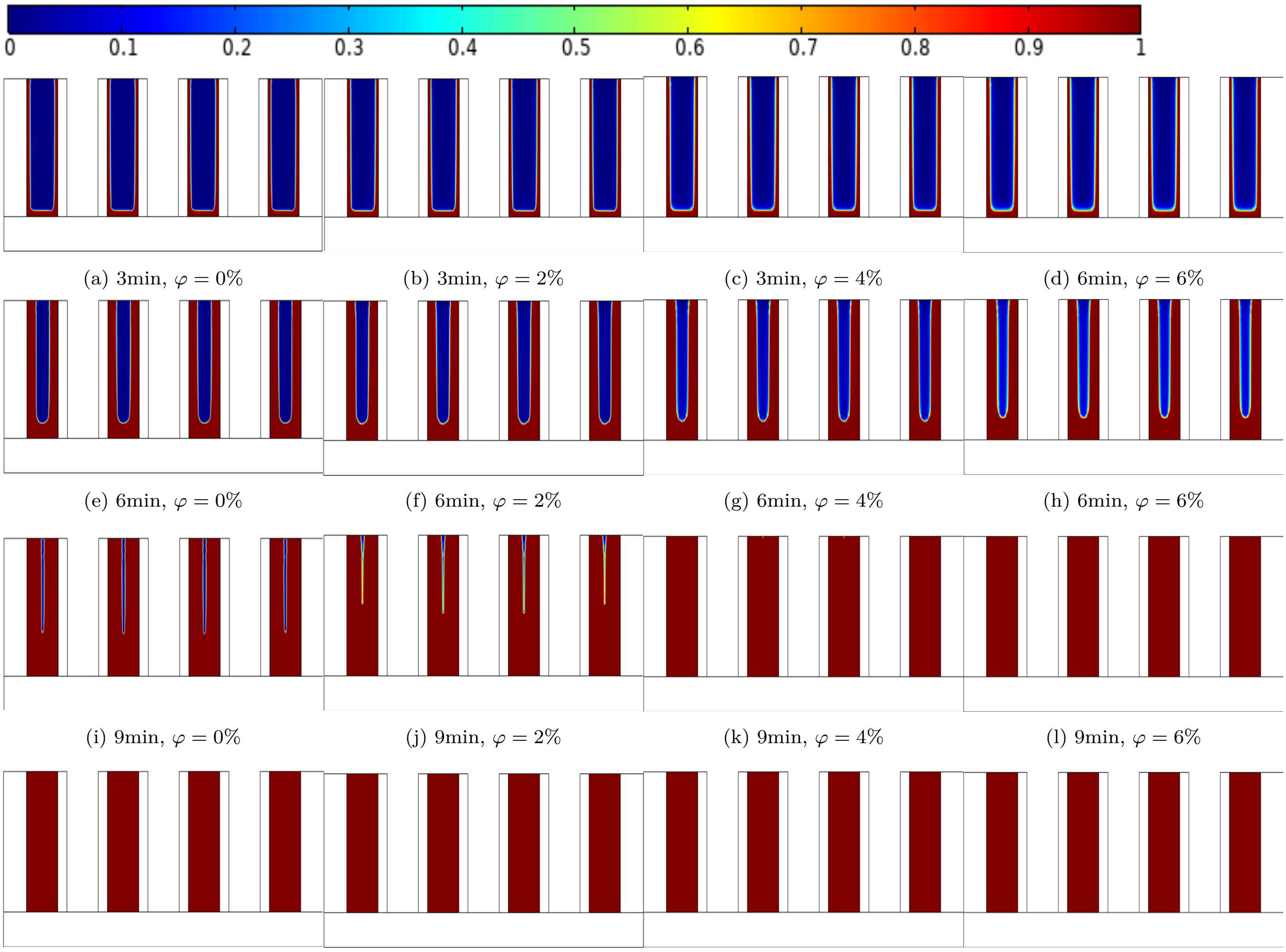

(a) 3min, $\varphi = 0\%$ (b) 3min, $\varphi = 2\%$ (c) 3min, $\varphi = 4\%$ (d) 6min, $\varphi = 6\%$

(e) 6min, $\varphi = 0\%$ (f) 6min, $\varphi = 2\%$ (g) 6min, $\varphi = 4\%$ (h) 6min, $\varphi = 6\%$

(i) 9min, $\varphi = 0\%$ (j) 9min, $\varphi = 2\%$ (k) 9min, $\varphi = 4\%$ (l) 9min, $\varphi = 6\%$

(m) 12min, $\varphi = 0\%$ (n) 12min, $\varphi = 2\%$ (o) 12min, $\varphi = 4\%$ (p) 12min, $\varphi = 6\%$

Figure 17: *Comparison of liquid fraction contours of hybrid HcPCM filled finned heat sink at* $\varphi = 0\%, 2\%$*,* 4% *and* 6% *and* h_c *= 10 W/m*^{2}*.K at various time-steps.*

transfer from the heat sink base to ambient and extends the latent heating phase of HcPCM due to the effective transfer rate. At $h_c = 100$ kW/m^2, there is no complete melting is achieved and heat sink temperature remains at ambient temperature even after 30 mins.

- The liquid fraction of HcPCM and Hybrid HcPCM heat sinks is increased with increase of volume fraction from 0% to 6%. Similarly, with $h_c = 10 - 100$ W/m^2.K, the higher liquid fraction is obtained from 100 to 10 W/m^2.K which means PCM does not melt fully.

It is concluded that the forced convection heat transfer improved the cooling performance of hybrid HcPCM finned heat sink compared to natural convection heat transfer in case of air-cooled and HcPCM finned-based heat sink. The addition of nanoparticles further enhanced thermal enhancement and uniform melting distribution of PCM inside the finned heat sink. The h_c between 30 to 50 $W/m^2.K$ shows the optimized values for forced convection heat transfer operating conditions. The volume fraction of 2% of GO+MWCNTs nanoparticles is recommended as an optimum concentration for uniform melting of PCM inside the finned heat sinks both for hybrid and non-hybrid cases.

Conflict of interest

The authors declare no conflict of interest regarding this research article.

References

References

[1] Thomas N Theis and H-S Philip Wong. The end of moore's law: A new beginning for information technology. *Computing in Science & Engineering*, 19(2):41–50, 2017.

[2] Scott E Thompson and Srivatsan Parthasarathy. Moore's law: the future of si microelectronics. *Materials today*, 9(6):20–25, 2006.

[3] Khellil Sefiane and Ali Koşar. Prospects of heat transfer approaches to dissipate high heat fluxes: Opportunities and challenges. *Applied Thermal Engineering*, 215:118990, oct 2022.

[4] I.M. Filanovsky and A. Allam. Mutual compensation of mobility and threshold voltage temperature effects with applications in CMOS circuits. *IEEE Transactions on Circuits and Systems I: Fundamental Theory and Applications*, 48(7):876–884, jul 2001.

[5] Liqiang Ding, Xiaowu Cai, Ruirui Xia, and Fazhan Zhao. A simplified over-temperature protection structure for smart power ICs. *Analog Integrated Circuits and Signal Processing*, 111(3):451–460, apr 2022.

[6] S.M. Sohel Murshed and C.A. Nieto de Castro. A critical review of traditional and emerging techniques and fluids for electronics cooling. *Renewable and Sustainable Energy Reviews*, 78:821–833, oct 2017.

[7] Adeel Arshad, Mark Jabbal, and Yuying Yan. Synthetic jet actuators for heat transfer enhancement – a critical review. *International Journal of Heat and Mass Transfer*, 146:118815, jan 2020.

[8] Zhihao Zhang, Xuehui Wang, and Yuying Yan. A review of the state-of-the-art in electronic cooling. *e-Prime*, page 100009, oct 2021.

[9] Adeel Arshad, Mark Jabbal, Yuying Yan, and Jo Darkwa. The micro-/nano-PCMs for thermal energy storage systems: A state of art review. *International Journal of Energy Research*, 43(11):5572–5620, may 2019.

[10] Y.S. See, J.Y. Ho, K.C. Leong, and T.N. Wong. Experimental investigation of a topology-optimized phase change heat sink optimized for natural convection. *Applied Energy*, 314:118984, may 2022.

[11] Muthamil Selvan Nedumaran, Gnanasekaran Nagarajan, and Kamel Hooman. Numerical analysis of multiple phase change materials based heat sink with angled thermal conductivity enhancer. *Journal of Energy Storage*, 55:105316, nov 2022.

[12] Ben Palmer, Adeel Arshad, Yan Yang, and Chuang Wen. Energy storage performance improvement of phase change materials-based triplex-tube heat exchanger (TTHX) using liquid–solid interface-informed fin configurations. *Applied Energy*, 333:120576, mar 2023.

[13] Shuai Zhang, Yuanpeng Yao, Yingai Jin, Zhen Shang, and Yuying Yan. Heat transfer characteristics of ceramic foam/molten salt composite phase change material (CPCM) for medium-temperature thermal energy storage. *International Journal of Heat and Mass Transfer*, 196:123262, nov 2022.

[14] Li Chen, An He, Jianlin Zhao, Qinjun Kang, Zeng-Yao Li, Jan Carmeliet, Naoki Shikazono, and Wen-Quan Tao. Pore-scale modeling of complex transport phenomena in porous media. *Progress in Energy and Combustion Science*, 88:100968, jan 2022.

[15] Shuai Zhang, Daili Feng, Lei Shi, Li Wang, Yingai Jin, Limei Tian, Ziyuan Li, Guoyong Wang, Lei Zhao, and Yuying Yan. A review of phase change heat transfer in shape-stabilized phase change materials (ss-PCMs) based on porous supports for thermal energy storage. *Renewable and Sustainable Energy Reviews*, 135:110127, jan 2021.

[16] M.A. Kibria, M.R. Anisur, M.H. Mahfuz, R. Saidur, and I.H.S.C. Metselaar. A review on thermophysical properties of nanoparticle dispersed phase change materials. *Energy Conversion and Management*, 95:69–89, may 2015.

[17] Liey-Si Wong-Pinto, Yanio Milian, and Svetlana Ushak. Progress on use of nanoparticles in salt hydrates as phase change materials. *Renewable and Sustainable Energy Reviews*, 122:109727, apr 2020.

[18] Adeel Arshad, Mark Jabbal, and Yuying Yan. Preparation and characteristics evaluation of mono and hybrid nano-enhanced phase change materials (NePCMs) for thermal management of microelectronics. *Energy Conversion and Management*, 205:112444, feb 2020.

[19] Ravi Kandasamy, Xiang-Qi Wang, and Arun S. Mujumdar. Transient cooling of electronics using phase change material (PCM)-based heat sinks. *Applied Thermal Engineering*, 28(8-9):1047–1057, jun 2008.

[20] S.C. Fok, W. Shen, and F.L. Tan. Cooling of portable hand-held electronic devices using phase change materials in finned heat sinks. *International Journal of Thermal Sciences*, 49(1):109–117, jan 2010.

[21] G. Setoh, F.L. Tan, and S.C. Fok. Experimental studies on the use of a phase change material for cooling mobile phones. *International Communications in Heat and Mass Transfer*, 37(9):1403–1410, nov 2010.

[22] Yue-Tzu Yang and Yi-Hsien Wang. Numerical simulation of three-dimensional transient cooling application on a portable electronic device using phase change material. *International Journal of Thermal Sciences*, 51:155–162, jan 2012.

[23] Yi-Hsien Wang and Yue-Tzu Yang. Three-dimensional transient cooling simulations of a portable electronic device using PCM (phase change materials) in multi-fin heat sink. *Energy*, 36(8):5214–5224, aug 2011.

[24] Rajesh Baby and C. Balaji. Experimental investigations on phase change material based finned heat sinks for electronic equipment cooling. *International Journal of Heat and Mass Transfer*, 55(5-6):1642–1649, feb 2012.

[25] Rajesh Baby and C. Balaji. Thermal optimization of PCM based pin fin heat sinks: An experimental study. *Applied Thermal Engineering*, 54(1):65–77, may 2013.

[26] Saad Mahmoud, Aaron Tang, Chin Toh, Raya AL-Dadah, and Sein Leung Soo. Experimental investigation of inserts configurations and PCM type on the thermal performance of PCM based heat sinks. *Applied Energy*, 112:1349–1356, dec 2013.

[27] Adeel Arshad, Hafiz Muhammad Ali, Muzaffar Ali, and Shehryar Manzoor. Thermal performance of phase change material (PCM) based pin-finned heat sinks for electronics devices: Effect of pin thickness and PCM volume fraction. *Applied Thermal Engineering*, 112:143–155, feb 2017.

[28] Hafiz Muhammad Ali, Adeel Arshad, Mark Jabbal, and P.G. Verdin. Thermal management of electronics devices with PCMs filled pin-fin heat sinks: A comparison. *International Journal of Heat and Mass Transfer*, 117:1199–1204, feb 2018.

[29] Hafiz Muhammad Ali and Adeel Arshad. Experimental investigation of n-eicosane based circular pin-fin heat sinks for passive cooling of electronic devices. *International Journal of Heat and Mass Transfer*, 112:649–661, sep 2017.

[30] Hafiz Muhammad Ali, Muhammad Junaid Ashraf, Ambra Giovannelli, Muhammad Irfan, Talal Bin Irshad, Hafiz Muhammad Hamid, Faisal Hassan, and Adeel Arshad. Thermal management of electronics: An experimental analysis of triangular, rectangular and circular pin-fin heat sinks for various PCMs. *International Journal of Heat and Mass Transfer*, 123:272–284, aug 2018.

[31] B. Debich, A. Yaich, K. Dammak, A. El Hami, W. Gafsi, L. Walha, and M. Haddar. Integration of multi-objective reliability-based design optimization into thermal energy management: Application on phase change material-based heat sinks. *Journal of Energy Storage*, 41:102906, sep 2021.

[32] Zilong Deng, Chengbin Zhang, Qing Sun, Liangyu Wu, Feng Yao, and Dehao Xu. Experimental study on melting performance of phase change material-based finned heat sinks by a comprehensive evaluation. *Journal of Thermal Analysis and Calorimetry*, 144(3):869–882, mar 2020.

[33] M Mozafari and Ann Lee. Thermal performance enhancement of a new dual-PCM heat sink using two-objective optimization. *Thermal Science and Engineering Progress*, 33:101383, aug 2022.

[34] M. Sivashankar and C. Selvam. Experimental investigation on the thermal performance of low-concentrated photovoltaic module using various pin-fin configurations of heat sink with phase change materials. *Journal of Energy Storage*, 55:105575, nov 2022.

[35] Rasool Kalbasi. Introducing a novel heat sink comprising PCM and air - adapted to electronic device thermal management. *International Journal of Heat and Mass Transfer*, 169:120914, apr 2021.

[36] B. Praveen, S. Suresh, and Vignesh Pethurajan. Heat transfer performance of graphene

nano-platelets laden micro-encapsulated PCM with polymer shell for thermal energy storage based heat sink. *Applied Thermal Engineering*, 156:237–249, jun 2019.

[37] Adeel Arshad, Mark Jabbal, Hamza Faraji, Pouyan Talebizadehsardari, Muhammad Anser Bashir, and Yuying Yan. Numerical study of nanocomposite phase change material-based heat sink for the passive cooling of electronic components. *Heat and Mass Transfer*, may 2021.

[38] Adeel Arshad, Mark Jabbal, Hamza Faraji, Pouyan Talebizadehsardari, Muhammad Anser Bashir, and Yuying Yan. Thermal performance of a phase change material-based heat sink in presence of nanoparticles and metal-foam to enhance cooling performance of electronics. *Journal of Energy Storage*, 48:103882, apr 2022.

[39] Faisal Hassan, Abid Hussain, Furqan Jamil, Adeel Arshad, and Hafiz Muhammad Ali. Passive cooling analysis of an electronic chipset using nanoparticles and metal-foam composite PCM: An experimental study. *Energies*, 15(22):8746, nov 2022.

[40] Hamza Fayyaz, Abid Hussain, Imran Ali, Hanzla Shahid, and Hafiz Muhammad Ali. Experimental analysis of nano-enhanced phase-change material with different configurations of heat sinks. *Materials*, 15(22):8244, nov 2022.

[41] Imran Zahid, M. Farhan, M. Farooq, M. Asim, and M. Imran. Experimental investigation for thermal performance enhancement of various heat sinks using al2o3 NePCM for cooling of electronic devices. *Case Studies in Thermal Engineering*, page 102553, nov 2022.

[42] Adeel Arshad, Mark Jabbal, Lei Shi, Jo Darkwa, Nicola J. Weston, and Yuying Yan. Development of TiO2/RT–35hc based nanocomposite phase change materials (NCPCMs) for thermal management applications. *Sustainable Energy Technologies and Assessments*, 43:100865, feb 2021.

[43] Adeel Arshad, Mark Jabbal, Hamza Faraji, Muhammad Anser Bashir, Pouyan Talebizadehsardari, and Yuying Yan. Thermal process enhancement of HNCPCM filled heat sink: Effect of hybrid nanoparticles ratio and shape. *International Communications in Heat and Mass Transfer*, 125:105323, jun 2021.

[44] J. Sunku Prasad, R. Anandalakshmi, and P. Muthukumar. Numerical investigation

on conventional and PCM heat sinks under constant and variable heat flux conditions. *Clean Technologies and Environmental Policy*, 23(4):1105–1120, mar 2020.

[45] Adeel Arshad, Mark Jabbal, Pouyan Talebizadeh Sardari, Muhammad Anser Bashir, Hamza Faraji, and Yuying Yan. Transient simulation of finned heat sinks embedded with PCM for electronics cooling. *Thermal Science and Engineering Progress*, 18:100520, aug 2020.

[46] Mohamed Fadl and Philip C. Eames. Numerical investigation of the influence of mushy zone parameter amush on heat transfer characteristics in vertically and horizontally oriented thermal energy storage systems. *Applied Thermal Engineering*, 151:90–99, mar 2019.

[47] Rasool Kalbasi, Masoud Afrand, Jalal Alsarraf, and Minh-Duc Tran. Studies on optimum fins number in PCM-based heat sinks. *Energy*, 171:1088–1099, mar 2019.

[48] Babak Kamkari and Hossein Shokouhmand. Experimental investigation of phase change material melting in rectangular enclosures with horizontal partial fins. *International Journal of Heat and Mass Transfer*, 78:839–851, nov 2014.

[49] Hamza Faraji, Mustapha El Alami, and Adeel Arshad. Investigating the effect of single and hybrid nanoparticles on melting of phase change material in a rectangular enclosure with finite heat source. *International Journal of Energy Research*, 45(3):4314–4330, oct 2020.

[50] Kenneth P. Wright, Joseph T. Hull, and Charles A. Czeisler. Relationship between alertness, performance, and body temperature in humans. *American Journal of Physiology-Regulatory, Integrative and Comparative Physiology*, 283(6):R1370–R1377, dec 2002.

[51] Adeel Arshad, Mark Jabbal, Lei Shi, and Yuying Yan. Thermophysical characteristics and enhancement analysis of carbon-additives phase change mono and hybrid materials for thermal management of electronic devices. *Journal of Energy Storage*, 34:102231, feb 2021.